Retention of arsenic, chromium and boron on an outcropping clay-rich rock formation (the Tégulines Clay, eastern France)

Mathieu Debure, Christophe Tournassat, Catherine Lerouge, Benoît Made, Jean-Charles Robinet, Ana María Fernández, Sylvain Grangeon

Retention of arsenic, chromium and boron on an outcropping clay-rich rock formation (the Tégulines Clay, eastern France)

Mathieu Debure[1,*], Christophe Tournassat[1,2,3], Catherine Lerouge[1], Benoît Madé[4], Jean-Charles Robinet[4], Ana María Fernández[5], Sylvain Grangeon[1]

[1] BRGM – French Geological Survey - 45060 Orléans - France.

[2] UMR 7327 Institut des Sciences de la Terre d'Orléans (ISTO), Université d'Orléans–CNRS/INSU–BRGM, Orléans, France

[3] Energy Geoscience Division, Lawrence Berkeley National Laboratory, 1 Cyclotron Rd., Berkeley, CA 94720, USA

[4] Andra, R&D Division, Transfer Migration Group, 92298 Châtenay-Malabry, France

[5] CIEMAT,Dpto. Medio Ambiente, Avda./Complutense 40, 28040, Madrid, Spain

Abstract

The retention behavior of three toxic chemicals, As, Cr and B, was investigated for an outcropping rock formation, the Albian Tégulines Clay (France, Aube). At a shallow depth, Tégulines Clay is affected by weathering processes leading to contrasted geochemical conditions with depth. One of the main features of the weathering is the occurrence of a redox transition zone near the surface. Batch sorption experiments of As(V), As(III), Cr(VI) and B were performed on samples collected at two depths representative either of oxidized or reduced mineral assemblages. Batch sorption experiments highlighted a distinct behavior between As, Cr and B oxyanions. Cr(VI) retention behavior was dominated by redox phenomena, notably its reduction to Cr(III). The *in-situ* redox state of the Tégulines Clay samples has a significant effect on Cr retention. On the contrary, As(V) reduction into As(III) is moderate and its retention slightly affected by the *in-situ* redox state of the Tégulines Clay. As(V) retention is higher than As(III) retention in agreement with literature data. B retention is strongly related to its natural abundance in the Tégulines clay samples. Distribution coefficient of B corrected from its natural content is expected to be very low for *in-situ* conditions. Finally, the retention and mobility of these oxyanions were affected by clay mineralogy, natural abundance, and reducing capacity of the Tegulines Clay.

***Keywords**: Oxyanions retention, Tégulines Clay, redox environment, arsenic, chromium, boron.*

[*] Corresponding author. E-mail address: m.debure@brgm.fr (M. Debure).

Graphical abstract

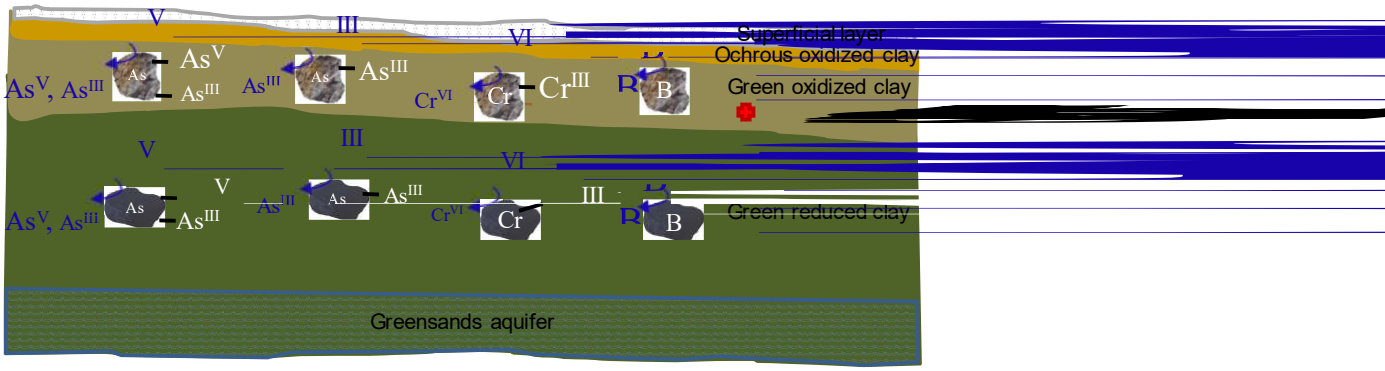

1. Introduction

Inorganic toxic chemicals occur in various forms (e.g., cations, oxyanions, and ligands). Among them, the oxyanionic forms are subject of high interest, because of their high mobility. In neutral conditions, the capacity of soils and sediments to retain anions and oxyanions is low compared to cations, because rock retention capacity is generally controlled by the presence of clay minerals and Fe and Mn oxyhydroxides, whose surface are negatively charged under most environmental conditions (Sparks, 2005). Limited retention through chemical reduction (Li and Bowman, 2001) or sorption on iron oxyhydroxides or clay minerals (Fendorf et al., 1997; Li, 1999) and oxidation by Mn oxides (James and Bartlett, 1983a; James and Bartlett, 1983b; Wu et al., 2018) have been reported in the literature for oxyanions. Therefore, the mobility of toxic chemicals is closely linked to the mineralogy of the sediments and to their oxidation-reduction (redox) potential. The variations of those parameters are significant in the critical zone, and may lead to discrepancies in the prediction of the behavior of toxic chemicals. The behavior of metals (Cu, Zn, Fe, Mn, Hg, Mo, etc.) in such a context has been extensively studied in the literature (Evans, 1989; Lynch et al., 2014; Nagajyoti et al., 2010; Poggio et al., 2009; Wuana and Okieimen, 2011) and references therein). In contrast, the mobility of inorganic toxic chemicals, with oxyanionic forms (AsO_4^{3-}, $H_2AsO_3^-$, $HAsO_3^{2-}$, AsO_3^{3-}, $B(OH)_4^-$, CrO_4^{2-}), sometimes combined with redox sensitivity (As(V)/As(III), Cr(VI)/Cr(III)) is less well understood.

The behavior of As and Cr depends on their oxidation state, which influences their solubility and the adsorption-desorption reactions on mineral surfaces. In the soil and water environment, inorganic As is mainly present in two oxidation states: arsenate (As(V)), which is predominant in oxidized environments, and arsenite (As(III)), which is predominant in reduced environments (Adriano, 1986; Arai, 2010; Gorny et al., 2015). Redox transformation rates for inorganic As species are slow, so As(V) and As(III) often co-exist in soil solutions (Masscheleyn et al., 1991; Tallman and Shaikh, 1980). The less toxic and less mobile oxidation state is As(V) (Arai, 2010; Goldberg and Johnston, 2001; Gulens et al., 1979; Penrose, 1974; Smedley and Kinniburgh, 2002). Usually, the extent of As uptake is positively correlated with clay mineral and extractable Fe and Al contents (Arai, 2010; Walsh and Keeney, 1975; Wauchope and McDowell., 1984). As(V) sorption on Al and Fe oxyhydroxides and on clay minerals exhibit sorption maxima in the pH range 3–7, while As(III) is retained between pH 7 and 9 (Goldberg, 2002; Goldberg and Johnston, 2001; Goldberg and Suarez, 2012; Jain and Loeppert,

2000). The mobility of As is thus a function of its oxidation state, the pH conditions and of the soil mineralogy. Cr is also a redox metal that can be encountered as Cr(III) or Cr(VI) in the environment (Gorny et al., 2016). These two oxidation states have contrasting toxicity and mobility: Cr(III) has very low toxicity and mobility in soils, while Cr(VI) is toxic and readily transported. The low Cr(III) solubility ($1.7\ 10^{-7}$ mol L^{-1} at pH 7 with respect to $Cr(OH)_{3(s)}$) limits its mobility and availability, while Cr(VI) is highly soluble in water (Ma and Hooda, 2010; Nakayama et al., 1981) and is mainly present in the environment as oxyanion species ($HCrO_4^-$ at pH < 6.5 and CrO_4^{2-} at pH > 6.5). Thus, the greatest risk associated with the presence of Cr(III) is its potential oxidation to Cr(VI), and this makes the presence of Cr(III) an environmental risk in the presence of fluctuant redox conditions (Fendorf, 1995; Ma and Hooda, 2010; Taghipour and Jalali, 2015). Manganese oxides, fly ash and hydroxyapatite affect Cr bioavailability by oxidizing Cr(III) to Cr(VI) (Bartlett and James, 1979; Pantsar-Kallio et al., 2001), while organic matter immobilizes Cr. Cr(VI) retention is higher at pH 7, because oxyanions are easily absorbed at positively charged sites on soil minerals. Indeed, the point of zero charge (pHzpc) for Fe- and Al- oxides varies from 7 to 10 (Alloway, 1995) generating positively charged adsorbent surface attracting anions. At higher pH than 8, a competition with OH^- hinders the sorption of oxyanions (Ma and Hooda, 2010). Considering their distinctive toxicity, determining Cr redox states, in the critical zones, such as close to aquifer, is of prime importance. B has no redox reactivity. B concentration in soils is controlled by adsorption reactions (Goldberg, 1997). B sorption capacity is strongly related to the organic and inorganic carbon content of the soil, as well as to the Fe oxyhydroxides (Goldberg et al., 2004) and to calcite content (Hemming et al., 1998). The highest B adsorption on clay minerals, organic matter, and calcite is produced at pH 8–10, while the highest sorption is reported at pH 7–9 on Al and Fe oxyhydroxides (Goldberg, 1997). This sorption is a two-step process with adsorption followed by incorporation. In clay minerals, B may replace Si and Al in tetrahedral sites (Couch and Grim, 1968; Fleet, 1965; Goldberg, 1997), while B uptake in calcite requires a change in B coordination from tetragonal ($B(OH)_4^-$) to trigonal ($B(OH)_3$) to be incorporated in its structure (Hemming et al., 1998; Mavromatis et al., 2015).

In many countries, environmental impact of toxic chemicals has to be considered for the implementation of industrial facilities. The assessment of the toxic chemical environmental impact for a given facility requires evaluating the mobility of the various toxic chemicals potentially involved in the industrial activity in its surrounding environment. Numerical evaluations of the migration of the

identified toxic elements from the industrial facilities toward the biosphere necessitate a good parametrization of their retention behavior. Long live low activity level (LL-LL) wastes include radium bearing wastes as well as toxic chemicals such as As, Cr and B not only from the nuclear power sector but also from the chemical industry (rare earth element extraction) and from cleanup waste radioactive contaminated sites (old industrial plants, laboratories…). The repository concept currently studied in France for LL-LL waste consists in a shallow depth repository (< 30 m) in a clay-rich geological formation. Since 2013, the Tégulines Clay, an Albian sedimentary formation in the eastern part of the Paris basin is currently under study for feasibility purposes. s , The ability of the Tégulines Clay to retain chemical elements, such as As, Cr and B was investigated. Due to its vicinity with the surface, the Tégulines Clay is affected by weathering processes inducing redox contrasts with depth (Lerouge et al., 2018). Such redox contrasts can potentially affect the mobility of sensitive redox chemical elements in the Tégulines Clay. Indeed, oxidized environment would sustain highly mobile oxyanions in the sediments (e.g. CrO_4^{2-}) while reduced environment would lead to their reduction and immobilization. Therefore, the retention behavior of As, Cr and B on samples originating from two depths with distinct redox environments was considered in this study to assess the mobility of these oxyanions and quantify the retention capacity of the Tegulines Clay.

2. Context of the study and samples

2.1. Geological setting

The marine Gault Clay Formation outcrops as an 8–10 km wide and 80-km long band of terrane oriented NE-SW through the Aube Department, in the eastern part of the Paris Basin (France) (Amédro et al., 2017; Lerouge et al., 2018). The Gault Clay is represented by Tégulines Clay in the study area of Brienne Le Chateau. Its thickness varies from 65-75 m to ~10 m. The Tégulines Clay is covered by thin (0.7 to 6 m thick) surficial layers of soils or alluvium. The mineralogy of the Tégulines Clay is mainly constituted by clay minerals (35-65 % including muscovite and/or illite, chlorite, kaolinite) associated with a quartz-feldspar silty fraction (18–58 wt.%), and carbonates (0–30 wt.%). Carbonates are essentially represented by calcite with minor dolomite. Ankerite and siderite were detected as well in the formation. Accessory minerals include pyrite, celestite, gypsum, phosphates nodules, and iron oxides. As the formation is being subjected to weathering with the occurrence of

oxidation phenomena, the mineralogy of the Tégulines Clay evolves with depth (see section 4.1 and Lerouge et al. (2018) for further details). Sulfur and iron bearing minerals are mainly affected by weathering that influences the mobility of the traces due to mineralogical modifications (see section 4.1).

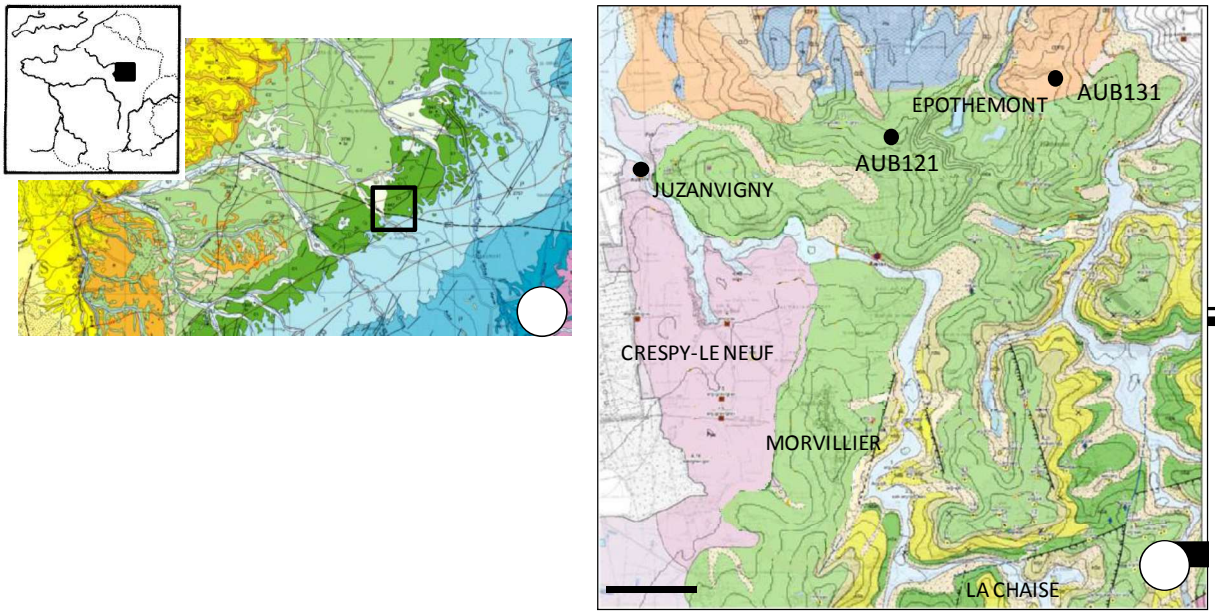

Fig. 1. Geological map (a) of the eastern part of the Paris Basin showing the investigated area; (b) zoom of the area studied and location of the boreholes.

2.2. Sampling

In order to define the impact of weathering processes on the As, Cr, and B distribution among minerals and on the retention capacity of Tégulines Clay, two core samples were selected according to depth. The AUB00976 sample was collected at 7.70 m depth of the borehole AUB121 crosscutting about 70 m of Tégulines Clay and the AUB00307 sample at 21.20 m depth of the borehole AUB131 crosscutting ~25-30 m of Tégulines Clay (Fig. 1). The AUB00976 and AUB00307 samples are considered as representative of the oxidized and reduced zones, respectively.

The two samples were packed and sealed within 10 to 30 minutes after their coring in double layer aluminum bags under vacuum to prevent any oxidation. Prior to packing, the samples were cut in rectangles parallel to the axis of the drill core to avoid any contamination by the drill mud. The aluminum bags were then opened in a glovebox under a nitrogen atmosphere. The blocks were roughly cut with a spatula covered with polytetrafluoroethylene, transferred in airtight containers and

frozen for 24 h at -45 °C. Finally, samples were freeze dried to remove water, then milled in an agate mortar, and sieved at 100 µm.

3. Materials and methods

3.1. Mineral characterization

3.1.1. *X-ray diffraction (XRD)*

XRD measurements were carried out on bulk-rock powder with a SIEMENS D5000 X-ray diffractometer with Co*Kα* radiation (λ = 1.79026 Å) operating at 50 kV and 50 mA. Samples were prepared using the RTS method (Zhang et al., 2003), and analyzed in step mode between 4 to 84° 2θ, with a counting time of 18 s per 0.04° step of 2θ. ICDD references for the different minerals of relevance for the present study are: quartz (00-046-1045), calcite (00-005-0586), muscovite (01-084-1302), kaolinite (01-078-1996), pyrite (00-042-1340), dolomite (01-084-2065), chlorite (00-046-1323), and microcline (01-084-1455).

3.1.2. *Electron microprobe*

Elemental mapping was carried on a CAMECA SXFiveFE electron microprobe equipped with a Schottky Field-Emission Gun (FEG) (CAMECA, Gennevilliers – France), using an acceleration voltage of 25 kV and beam current of 40 nA for Fe, Ca, and Mn, and an accelerating voltage of 25 kV and a beam current of 288 nA for As and S. As*Lβ* was measured on large thallium acid phthalate (LTAP), S*Kα* and Ca*Kα* on large pentaerythritol (LPET), Mn*Kα* on large lithium fluoride (LLIF), and Fe*Kα* on lithium fluoride (LiF).

Fully quantitative compositional spot analyses of silicates (clay minerals, feldspar), carbonates, pyrite, sulfates (gypsum and celestite), phosphates, and iron-hydroxides were carried out at BRGM using a Cameca SXFive electron microprobe with an accelerating voltage of 20 kV and a beam current of 100 nA. Na*Kα*, As*Lα* and Sr*Lα* were measured on LTAP, Mg*Kα*, Al*Kα* and Si*Kα* on TAP, S*Kα*, Ca*Kα*, K*Kα* on PET, Cr*Kα* and Mn*Kα* on LPET, and Fe*Kα* on LiF. Counting times on peaks and backgrounds were 10 s for Na, Mg, S, and Mn, 30 s for Al, Si, Ca, K, Cr, and Fe, and 60 s for As. The system was calibrated with a variety of natural minerals (albite for Na, andradite for Si and Ca, pyrite for Fe and S, orthoclase for K), synthetic oxides (MgO for Mg, Al_2O_3 for Al, $MnTiO_3$ for Ti, and $SrSO_4$ for Sr), metal

alloy (AsGa for As) and pure elements (Cr). Matrix corrections were made with the phi-rho-Z computing program PAP (Pouchou and Pichoir, 1984).

3.2. Natural contents and distribution of As, Cr, and B among phases in Tégulines Clay

The natural abundance of As, Cr, and B in the samples was measured after a tri-acid attack on bulk powder (HCl, HNO_3, HF) by ICP-MS, and their distribution among the chemical reservoirs was discriminated after sequential extractions. Sequential extractions were made on triplicates of each sample in a glove box following the method developed by Claret et al. (2010), modified after Tessier et al. (1979) (see Supplementary information A for details on extractants and mineralogical targets).

3.3. Pore water extracted by squeezing

Pore water was extracted from the clay samples by squeezing according to a method adapted from Fernández et al. (2014). A modification of the water sampling circuit was made for extracting the pore water at anoxic conditions, preserving its redox state. In addition, pore water chemistry was calculated following the method developed by Gaucher et al. (2009) for the Callovian-Oxfordian host rock, a claystone which is studied for the disposal of high level radioactive waste. The squeezing measurements were carried out only on the reduced sample, which was less exposed to atmospheric perturbations than the oxidized sample. The pore water was, therefore, not or less disturbed by rock oxidation. The mass of the core sample was measured before and after squeezing. The initial mass of core samples ranged between 300 and 500 g. Extractions were carried out at 10 MPa over seven days.

3.4. Analysis of the aqueous phases

The measurement of pH in batch solutions was carried out with a Metler Toledo, SevenMulti pH meter using NIST 1.7, 4, 7, and 9 buffers. Inductively coupled plasma atomic emission spectroscopy (ICP-AES, Jobin Yvon) or mass spectroscopy (ICP-MS, Thermo Fisher Scientific) were used to measure B, As, Ca, K, Mg, Na, and Si concentrations. Chloride anions were analyzed by ionic chromatography (HPLC, Dionex). The elemental concentrations in solution were determined with a relative uncertainty of 3 %. Alkalinity was measured using a Titrando 905 and a Dosino 800 equipped with a 5 mL syringe (Metrohm) to inject the HCl solution (10^{-3} mol L^{-1}) in the sample. The alkalinity was then calculated with

the Gran method (Gran, 1952). As speciation was determined using High-performance liquid chromatography (HPLC) coupled with an AFS-HG (Atomic Fluorescence Spectrometry-hydride generation) called Xcalibur (Thermo Fisher) or by ICP. In the first case, the solution is analyzed straightaway (typically within 15 min), while in the second case, As(V) was separated from As(III) on resin (Biorad AG 1X8, 50-100 Mesh), and then As(V), As(III), and total As were analyzed to check the results consistency. The recovery percentage was 100 ± 5 %. Ultraviolet/visible spectrophotometry (UV-VIS) of Cr(VI) was done conforming to the ISO 11083 international standard with an ATI Unicam UV2 spectrophotometer.

3.5. Preparation of the synthetic water

The synthetic pore water was prepared with boiled and outgassed Millipore Milli-Q® 18 MΩ water and using $CaSO_4{:}2H_2O$, $MgSO_4{:}7H_2O$, KCl, NaCl, $SrCl_2{:}6H_2O$, Na_2SO_4 and $NaHCO_3$ analytical grade salts (Supplementary information B). The preparation was done in a glove box with an atmosphere closed to the field, and equilibrated with carbonates (99 % N_2 / 1 % CO_2). The synthetic pore water chemistry was based on pore water chemistry modeled in Tégulines Clay from the drilling campaigns described in Lerouge et al. (2018), following the procedure given by Gaucher et al. (2009) for the Callovian-Oxfordian clay rock. *In situ* pore water measured by squeezing (Lerouge et al., 2018) was consistent with the model and validated it. Synthetic pore water was used in this study for the equilibration and "batch" sorption tests in order to reach the steady state concentrations of major elements faster than by addition of Milli-Q® 18 MΩ water and avoid mineral dissolution.

3.6. Determination of natural contents of As, Cr and B release from Tégulines Clay and sorption tests

All the experiments were done in a glove box under anoxic conditions to avoid on one hand the oxidation of the sediments, and on the other hand the oxidation of the redox sensitive toxic elements. Once the pore water had been prepared, the desired volume was equilibrated with a suitable sediment mass in a polypropylene copolymer (PPCO) container for at least 24 h under agitation. Once the time limit had been reached, the agitation was stopped, the solution was decanted for 30 min, and then the supernatant was sampled, filtered at 0.1 µm, and acidified with 20 µL of HNO_3 suprapur®.

Three types of experiments were conducted for best understanding of the behavior of As, Cr, and B in the Tégulines Clay rock formation. They consisted of: (i) kinetics equilibration experiments, which aimed at determining the equilibrium concentration of As, Cr, and B in the pore water, as well as determining the kinetics of equilibration between the sediments and the solution; (ii) batch sorption tests, which aimed at determining the As, Cr, and B distribution coefficients on the sediments; and (iii) kinetics sorption experiments, which aimed at determining the kinetics of As and Cr sorption on the sediments. Thus, As, Cr, or B were only spiked in the solutions for the (ii) and (iii) experiments.

To determine the natural release of As, Cr, and B from the Tégulines Clay, and thus the equilibrium concentrations, kinetic experiments were completed over 49 days at a solid to liquid ratio (R_{SL}) of 1 g L^{-1}. Measurements were performed on independent experiment samples at 8, 9, 26, 42, and 49 days. For each contact time, three replicates were analyzed. In addition, equilibration experiments were done at an R_{SL} ranging from 0.001 to 0.1 kg L^{-1}, and with pH values in the range of 7.2–7.4, to better constrain the natural source.

Sorption tests were conducted at an R_{SL} of 10 g L^{-1}. Mother solutions containing the element of interest (As, Cr, or B) were prepared with analytical grade salts (using $Na_2HAsO_4.7H_2O$, $NaAsO_2$, Na_2CrO_4 or $Na_2B_4O_7.10H_2O$). Then, an aliquot was introduced into a vial containing the sediment suspension in order to reach the initial target concentration. The solution and the sediments were kept in contact for at least four days. Sampling of the reacted sediments and solution was the same as the one described for the equilibration tests.

Kinetic sorption experiments were made for redox sensitive elements (As and Cr) at the following sample time: 1, 7, 15, and 30 days. The method was the same as the one described above. Two Cr(VI) concentrations have been tested (5.1 10^{-6} and 4.8 10^{-5} mol L^{-1}) due to the high concentration decrease observed with the lowest concentration, while only one was tested for As(V) (2.5 10^{-5} mol L^{-1}). Two replicates were made for each sample time. The fact that the added concentrations remain under the solubility of potential phases was checked with Phreeqc program (Parkhurst and Appelo, 2013) using the Thermoddem (Blanc et al., 2012) and ThermoChimie databases (Giffaut et al., 2014).

4. Results

4.1. Mineral and chemical characterization of oxidized and reduced Tégulines Clay samples

The AUB00307 sample of Tégulines Clay consisted of ~57 wt.% clay minerals, ~9 wt.% carbonates, and 32 wt.% quartz-feldspar (Table 1). The AUB00976 sample consisted of ~56 wt.% clay minerals, ~16.5 wt.% carbonates, and 26 wt.% quartz-feldspar (Table 1). Variation in carbonate content and quartz-feldspar content was essentially due to the position of the sample in the clay formation (Fig. 2 a). The clay fraction was quite similar in the both samples, and essentially consisted of illite/mica and illite-smectite mixed layers with minor amounts of kaolinite and chlorite. The carbonate fraction was essentially composed of calcite with minor amounts of dolomite and siderite. Pyrite was detected by XRD in the AUB00307 reduced sample, but not in the AUB00976 oxidized sample.

Complementary microscopic optical observations indicated that a large part of the calcite occurs as bioclasts (ammonites, foraminifers) (Fig. 3d & g), micrite disseminated in the clay matrix, and minor microsparite filling some bioclasts or cementing quartz grains. Diagenetic glauconite was frequently observed as 20 to 50 µm-sized aggregates, always green in color in the AUB00307 sample (Fig. 3f & h), but green to brownish in color in the AUB00976 sample (Fig. 3c). Pyrite usually occurred as < 10 µm sized framboids disseminated in the clay matrix and as a filling in bioclasts and bioturbations (Fig. 3g & h). In the AUB00976 sample, pyrite was replaced by brownish iron oxyhydroxides (Fe-Ox) and gypsum. Gypsum also occurred as 100-500 µm sized euhedral grains (Fig. 3e). As expected, the mineral assemblage of the AUB00976 sample gave evidence of oxidation (glauconite changes, pyrite dissolution, iron hydroxides and gypsum precipitation) while AUB00307 remained reduced (glauconite still green, pyrite, no iron hydroxides or gypsum).

Table 1 Quantification of the mineralogical composition of the oxidized sample (AUB00976) and reduced sample (AUB00307) by XRD (data in wt.%). Names in italics refer to the drilling described in Fig. 1 and in Lerouge et al. (2018).

		AUB00976 *(AUB121)*	**AUB00307** *(AUB131)*
Depth		7.8–7.95 m	21.75–21.93 m
Phyllosilicates	Chlorite/vermiculite	3.8	1.3
	Illite/mica	20.2	22.7
	Illite/Smectite interstratified	24.0	21
	Kaolinite	8.0	12.4
	Sum	56.0	57.4
Carbonates	Calcite	16.2	8.9
	Dolomite/ankerite	0.2	0.2
	Siderite	0.1	0.3
	Sum	16.5	9.4
Tectosilicates	Feldspar	3.5	3.8
	Quartz	22.6	27.9
	Sum	26.1	31.7
Oxides	Anatase	0.7	0.8
	Rutile	0.3	0.1
Sulfurs	Pyrite	0	0.4

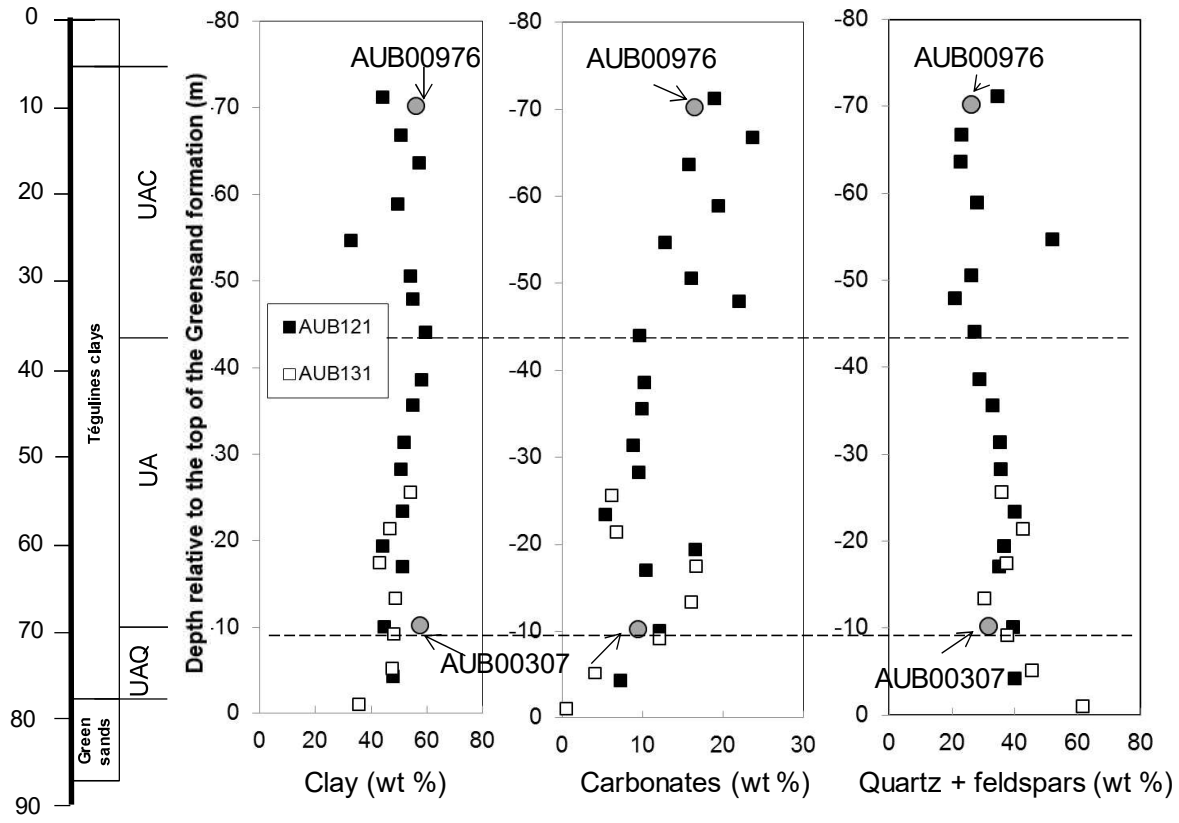

Fig. 2. Profiles of clay minerals, carbonates, and quartz + K-feldspar contents as a function of depth relative to the top of the greensands. Dashed lines indicate the limits of the three units defined in the Tégulines Clay. The positions of the two samples are indicated in each profile according to the Figure 2 in Lerouge et al. (2018).

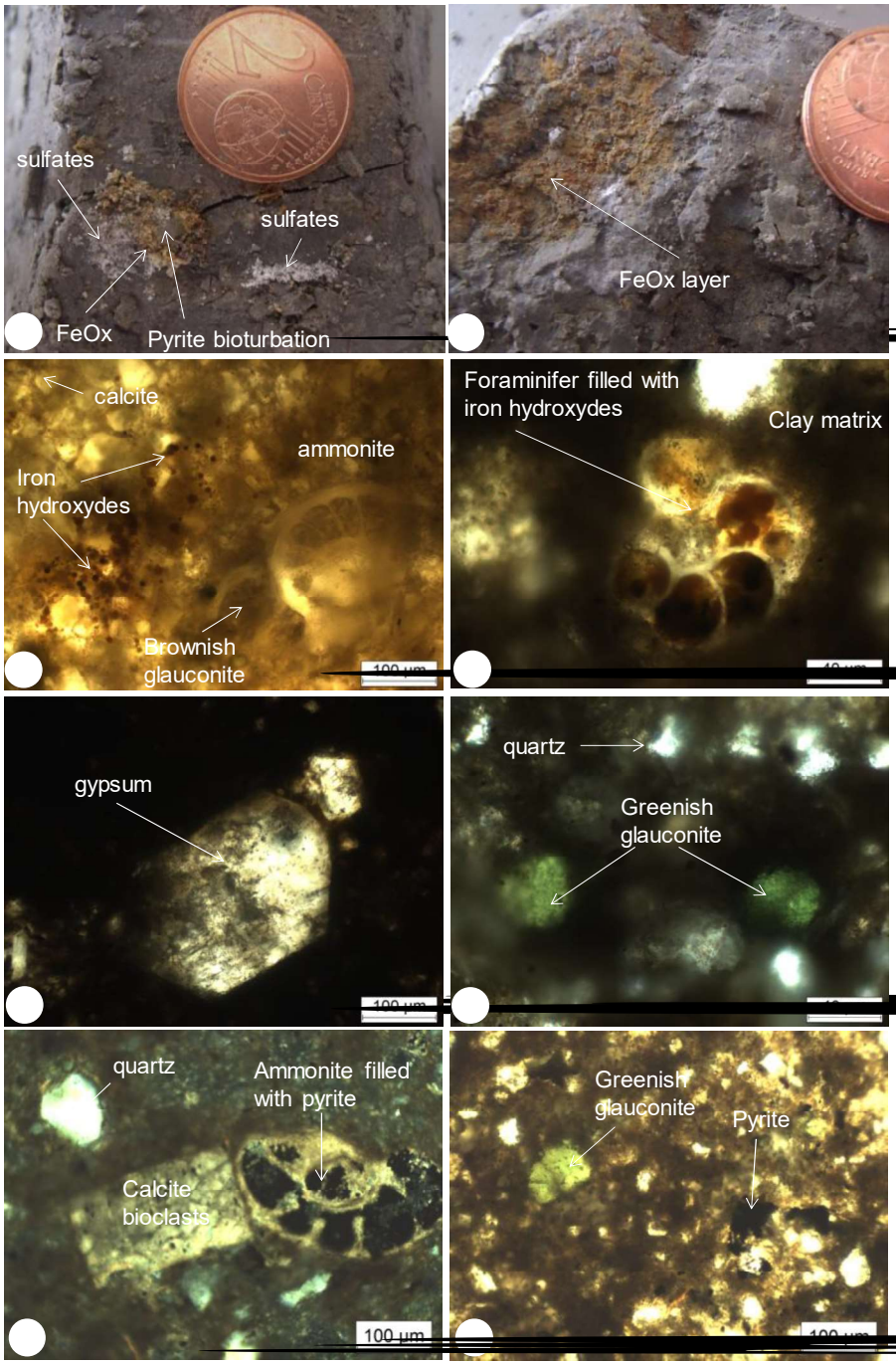

285

286 **Fig. 3. Photographs of: (a) oxidized sample in which pyrite bioturbation, FeOx and sulfates can**
287 **be observed; (b) FeOx layer in oxidized sample; and photomicrographs (in transmitted light) of:**
288 **(c) calcite, ammonite, iron hydroxides and altered brownish glauconite (oxidized sample); (d)**
289 **foraminifer filled with iron hydroxides in the clay matrix (oxidized sample); (e) gypsum**
290 **(oxidized); (f) well preserved rounded, green mass of glauconite and quartz (reduced); (g)**
291 **quartz, calcite and ammonite filled with pyrite (reduced sample); (h) well preserved rounded,**
292 **green mass of glauconite and pyrite (reduced sample).**

4.2. Distribution of trace elements (As, Cr, B) among phases of Tégulines clay samples

Sequential extractions were conducted in order to determine the natural distribution of the studied elements among the mineral phases (Fig. 4), and bulk (As, Cr, B) contents of studied samples were compared with bulk (As, Cr, B) element contents of tégulines Clay from drilling campaigns described in Lerouge et al. (2018) (Fig. 5).

The abundance of As in the exchangeable fraction was low (< 0.3 %) in the two samples (Fig. 4a). Similarly, As was only present in trace amounts in carbonates (0.7 ± 0.2 % and 0.8 ± 0.03 % for reduced and oxidized samples, respectively), and in Fe and Mn oxyhydroxides (1.0 ± 0.2 % and 0.9 ± 0.1 % for reduced and oxidized samples, respectively). In contrast, organic matter was a larger reservoir of As for the reduced sample (11.4 ± 1.2 %) than for the oxidized sample (1.4 ± 0.1 %). In both samples, the residual fraction was the main As reservoir. The As contents did not vary significantly with depth in the Tegulines Clay, but varied between boreholes (Fig. 5). The As concentrations measured in the reduced sample (21.2 ± 3.9 µg g^{-1}) were higher than those measured in the oxidized sample (13.9 ± 0.8 µg g^{-1}), although both remained in the range of values for the Tégulines Clay (51 ± 31 µg g^{-1}) (Fig. 4).

The total Cr concentrations were 111.1 ± 8.7 µg g^{-1} in the reduced sample and 117.2 ± 15.2 µg g^{-1} in the oxidized sample, and was found to be heavily concentrated in the residual fraction (Fig. 4b). Those values were close to the average concentrations reported in the Tégulines Clay for Cr (109 ± 37 µg g^{-1}) (Fig. 5). The highest extraction yields were obtained in the fraction corresponding to organic matter (2.4 ± 0.2 % in the reduced sample and 1.6 ± 0.2 % in the oxidized sample). It is noteworthy that Fe and Mn oxyhydroxides retained an order of magnitude more Cr in the reduced sample (0.80 ± 0.04 %) than in the oxidized sample (0.07 ± 0.02 %).

The B concentrations were 96.5 ± 4.7 µg g^{-1} and 117.3 ± 5.6 µg g^{-1} for the reduced and oxidized samples, respectively. Those values were close to the average concentrations reported in the Tégulines Clay for B (111 ± 22 µg g^{-1}) (Fig. 5). In both samples almost all of the B (> 98 %) was concentrated in the residual fraction (Fig. 4c).

Electron microprobe analyses of pyrite, iron hydroxides, gypsum, celestite, calcite, glauconite, and clay matrix indicated that As was essentially detected in pyrite (628 ± 240 µg g^{-1}, n = 27), iron-

hydroxides (211 ± 307 µg g^{-1}, n = 20), and gypsum (170 µg g^{-1}), whereas Cr was detected essentially in glauconite (564 ± 288 µg g^{-1}, n = 30), clay matrix (188 ± 33 µg g^{-1}, n = 20), and also in phosphates (114 ± 106 µg g^{-1}, n = 5). Additionally, iron hydroxides produced from oxidation of pyrite were richer in As (609 ± 181 µg g^{-1}, n = 9) than iron hydroxides in the clay matrix (As was below the detection limit of 150 µg g^{-1}).

Complementary X-ray dot mapping of As from a zone of oxidized pyrite surrounded by iron hydroxides and gypsum using the electron microprobe confirmed that As occurs as a trace element in pristine pyrite, secondary gypsum, and iron hydroxides, but not in the clay matrix (Fig. 6).

330

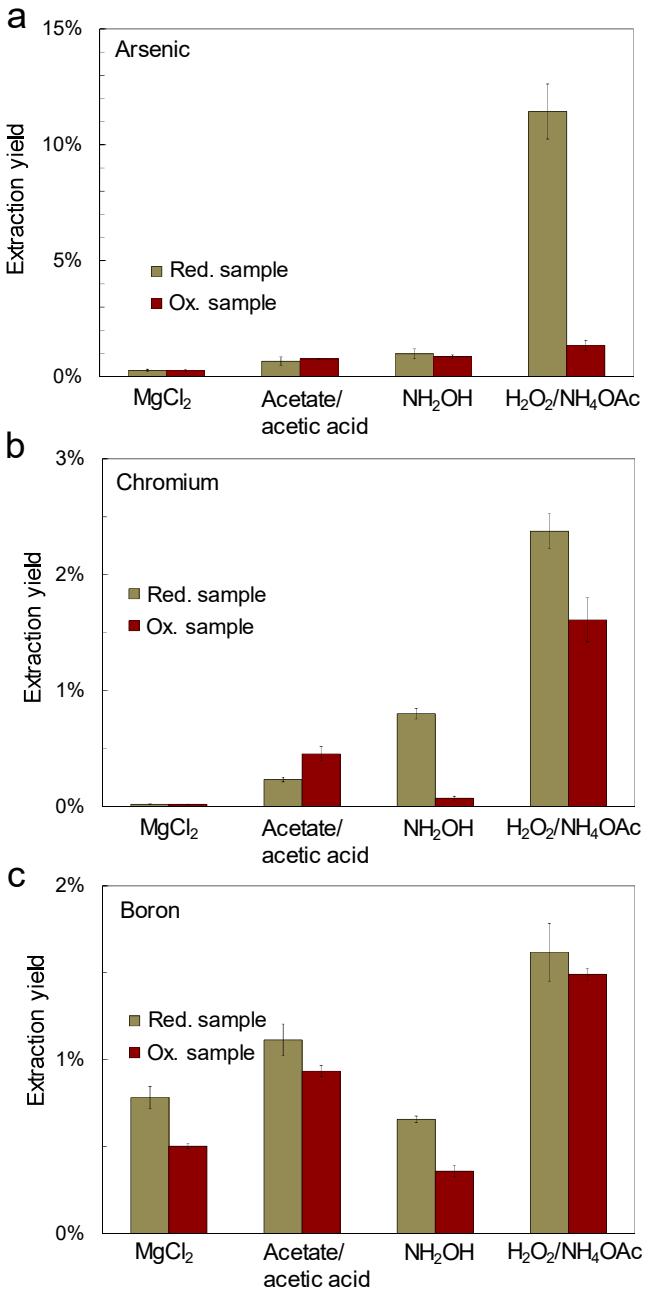

331

332 **Fig. 4. Percentages of As (a), Cr (b), and B (c) at each step of the sequential extraction of the**
333 **reduced (AUB00307) and the oxidized (AUB00976) Tégulines clay samples. The four fractions**
334 **correspond to exchangeable, carbonate, Fe-Mn-oxyhydroxides, and organic matter, while the**
335 **residual fraction is not shown. The error bars were calculated using three replicates of the**
336 **experiments.**

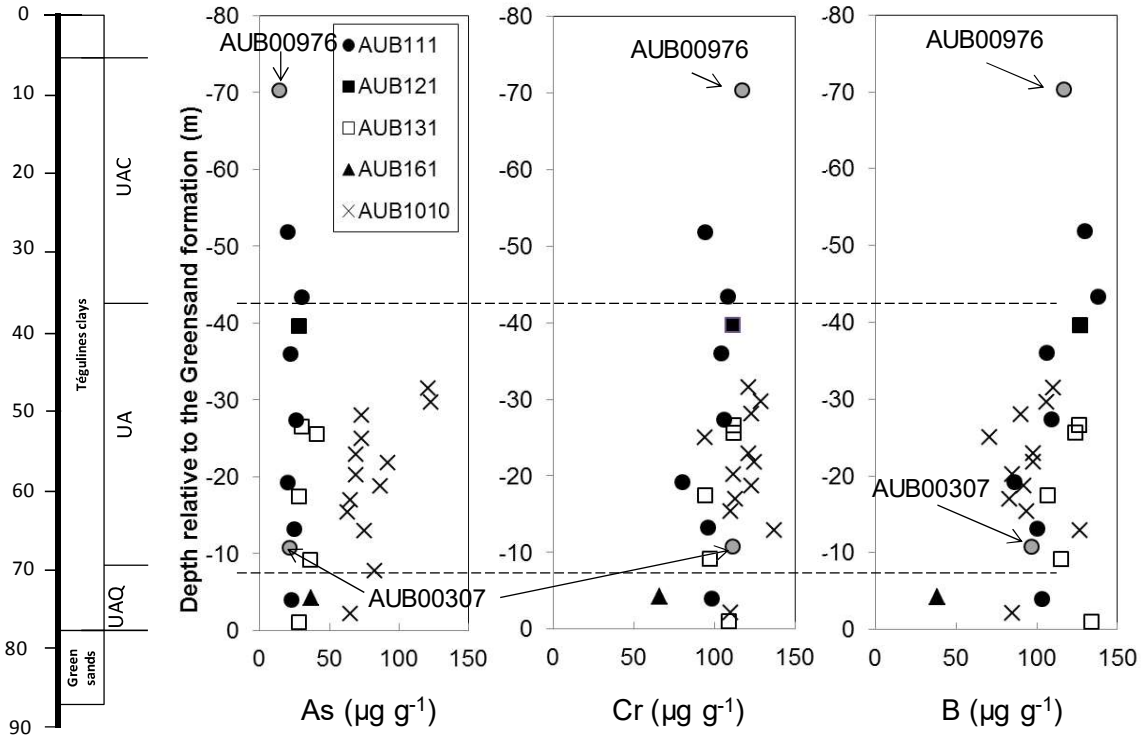

Fig. 5. Profiles of As, Cr and B contents as a function of depth relative to the top of the greensands. Dashed lines indicate the limits of the three units defined in the Tégulines Clay. The positions of the two samples are indicated in each profile according to the Figure 2 in Lerouge et al. (2018).

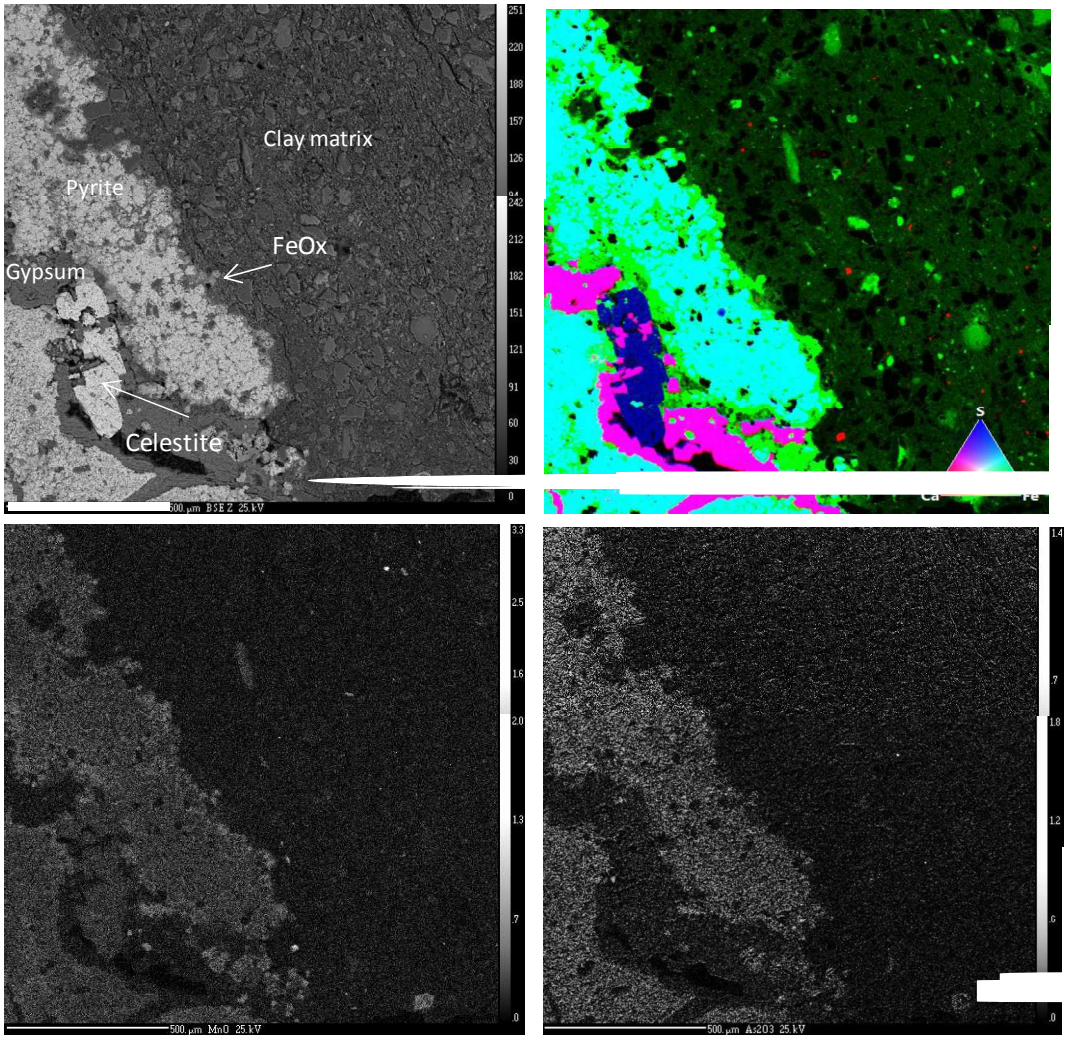

Fig. 6. Reactive assemblage observed in the transition redox zone (AUB1010, depth 8.25 m) showing early diagenetic celestite and pyrite partially oxidized into iron oxides and gypsum: (a) BSE image; (b) Ca- Fe-S ternary RGB map; (c) Mn X-ray dot map; and (d) As X-ray dot map.

4.3. Chemical composition of pore waters extracted by squeezing

Pore waters were extracted by squeezing technique from the reduced sample (Table 2). The pH value of the extracted pore waters was measured at 7.7, and a carbonate alkalinity value at 3.7 meq L^{-1}. The calculated ionic strength was 0.1. The concentrations of Ca, Mg and sulfate were the greatest in the pore waters. The $S_2O_3^{2-}$ concentration (0.20 mmol L^{-1}) is consistent with the reduced state of the sample. Both Fe and Al were systematically below the detection limit (0.01 mmol L^{-1}).

356 **Table 2.** Pore water chemistry measured after squeezing of the reduced sample (in mmol L^{-1}).

Anions	Cl^-	SO_4^{2-}	$S_2O_3^{2-}$	Br^-	NO_3^-	PO_4^{3-}	F^-	
(mmol L^{-1})	1.47	26.02	0.20	0.002	< 0.016	0.018	0.034	
Cations	Si	Na	K	Mg	Ca	Ba	Sr	Fe
(mmol L^{-1})	0.2	2.78	1.38	16.87	16.57	< 0.002	0.42	< 0.005
Trace elements	As	B	Cd	Cr	Cu	Hg	Mn	Zn
(µmol L^{-1})	0.01	148	0.003	0.029	58	0.015	29	31

357

358 *4.4. Sample equilibration and element natural release in solution*

359 Equilibration experiments revealed that in the two samples, As is principally released in solution as
360 As(III) (Fig. 7), which was detected in all replicates of equilibration tests made with the reduced
361 sample. As(V) was only detected at 9 and 42 days in two replicates with the oxidized sample. The
362 detected values remained lower than As concentration in the pore water (10^{-8} mol L^{-1}, see Fig. 7 and
363 Table 2 for pore water value) although two replicates evidenced higher concentration after 8 days of
364 equilibration. The concentrations remained almost stable during the experiments pleading for a quick
365 equilibration of the system with labile As.

366 The measured Cr concentrations in solution (i.e. Cr_{total} and Cr(VI)) remained negligible in the time
367 scale investigated here (< 1.9 10^{-9} mol L^{-1}), and therefore, they were lower than those found in the
368 squeezed pore water (2.9 10^{-8} mol L^{-1}, see Table 2).

369 The measured B concentrations were constant with time and were similar in the two samples. The
370 values were 30 times lower than those for the squeezed pore water (1.5 10^{-4} mol L^{-1}).

371

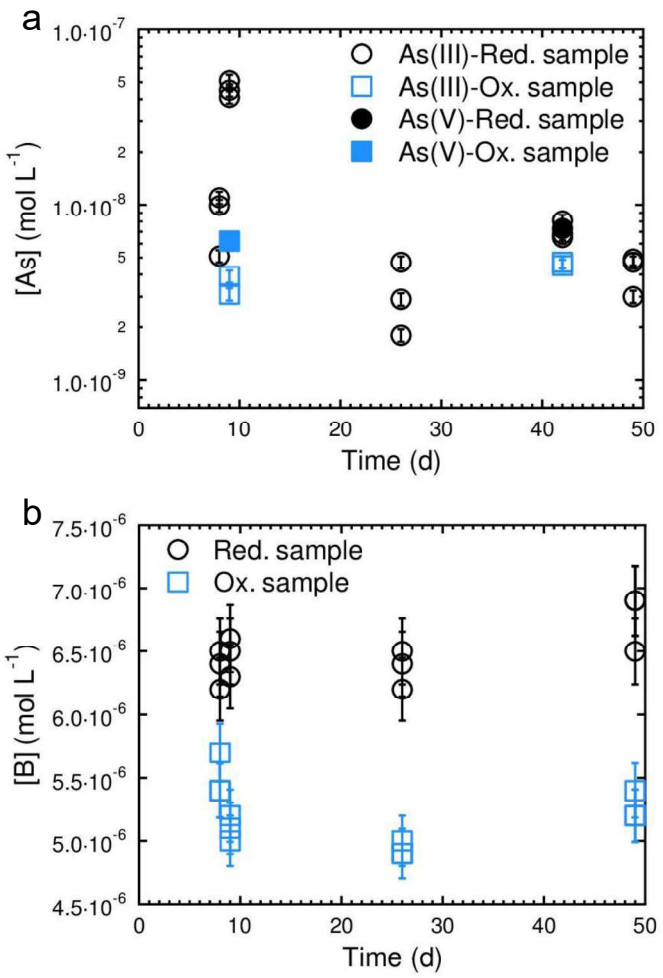

372

373 **Fig. 7. As (a) and B (b) concentrations during the kinetic equilibration of the oxidized sample**
374 **(AUB00976) and reduced sample (AUB00307) of Tégulines Clay. Analytical uncertainties are 4**
375 **%, and As and B quantification limit (QL) were 7 10^{-10} mol L^{-1} and 4.6 10^{-8} mol L^{-1}, respectively.**
376 **For a same time, the different circles and squares were replicates.**

377 Cr was undetectable (< 1.9 10^{-9} mol L^{-1}) in the equilibration tests performed from 0.001 to 0.1 kg L^{-1},
378 while As concentrations ranged from 2 10^{-9} to 8 10^{-9} mol L^{-1}, and were independent of the solid to
379 liquid ratio (R_{SL}). In contrast, B concentrations increased with R_{SL} (Fig. 8). The B concentrations
380 remained slightly higher in reduced samples as compared to oxidized samples, consistent with the
381 kinetics experiments (Fig. 7). The boron released in solution as a function of the solid/liquid ratio
382 enabled determination of the labile concentration for each sample, as well as the initial distribution
383 coefficient (see Section 5.3).

384

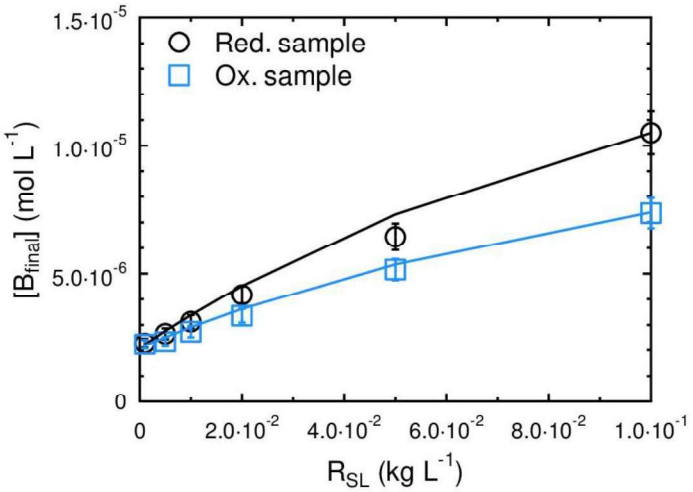

385

386 **Fig. 8. B concentrations in solution (mol L^{-1}) are a function of the solid to liquid ratio (R_{SL} in kg**
387 **L^{-1}). The solid lines represent the fits obtained according to Equation 7 (see section 5.3).**

388 *4.5. Sorption experiments on Tégulines Clay*

389 4.5.1. *Arsenic*

390 As in solution remained mostly in its As(V) form in solution while in contact with the reduced or
391 oxidized samples of Tégulines Clay (Fig. 9). An initial reduction occurred and led to the formation of
392 As(III), but this seemed to stop after one day of reaction. Within 1 day, 60 % of the As was adsorbed,
393 before the sorption slowed down according to a first order law. At the end of the experiments, 25 % of
394 the As was still present in solution.

395 Upon adsorption, As(V) was reduced to As(III), and the release of As(III) in solution was revealed
396 during the equilibration tests. Thus, sorption tests with As(III) were done in order to better constrain the
397 rock capacity to retain this form of As. The results showed a slightly higher As retention on the
398 oxidized sample than on the reduced sample (Supplementary information C). In both cases, the
399 retention was significant and ranged from 20 to 60 % for the oxidized sample and from 15 to 50 % for
400 the reduced sample.

401

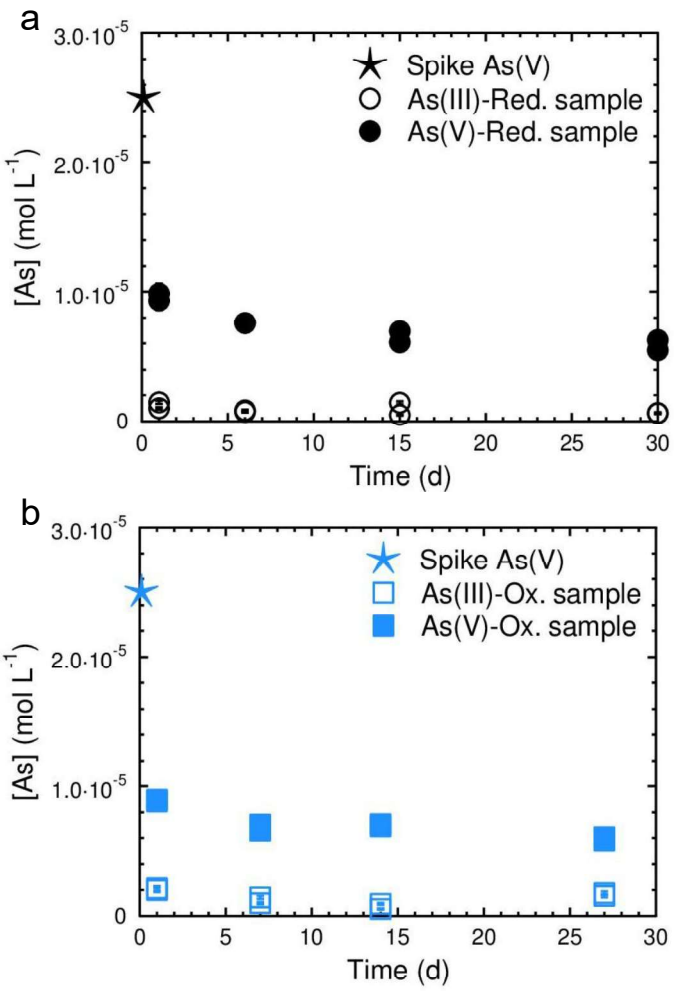

402

403 **Fig. 9. As speciation (As(V) and As(III)) in the kinetic experiment of sorption with an initial**
404 **concentration of 2.5 × 10^{-5} mol L^{-1} in contact with: (a) the reduced sample (AUB00307); (b) the**
405 **oxidized sample (AUB00976).**

406 4.5.2. *Chromium*

407 Cr sorption experiments were performed using Cr(VI), because it is its expected form during its
408 release from the (LL-LL) radioactive waste. The introduction of 4.8 10^{-5} mol L^{-1} Cr(VI) in a suspension
409 was followed by a fall of Cr(VI) in solution until 2.7 10^{-6} mol L^{-1} (Fig. 10a). This decrease occurred
410 within 30 d of the interaction with the reduced sample, and represented a loss of 95 % of the Cr(VI),
411 while only 20 % was removed in the case of the oxidized sample (Fig. 10a). The difference was higher
412 for the lowest tested concentrations (5.1 10^{-6} mol L^{-1}). In contact with the reduced sample, Cr(VI) was
413 removed from the solution between 1 and 6 days (Fig. 10b), while only 25 % (3.7 10^{-7} mol L^{-1}) of the
414 Cr(VI) remained in solution in contact with the oxidized sample (Fig. 10b).

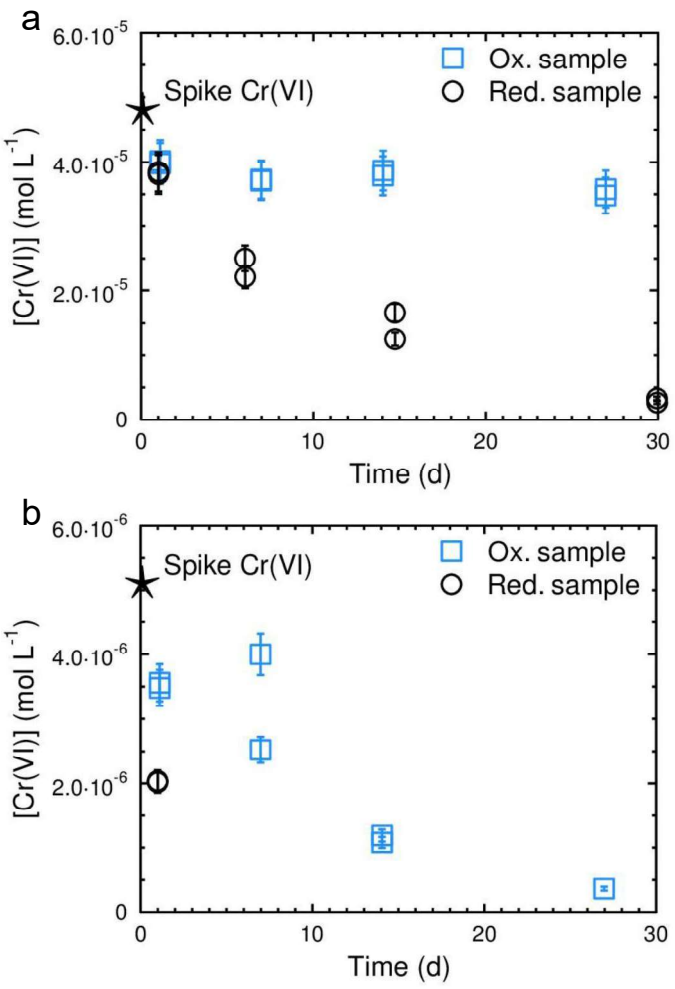

415

416 **Fig. 10. Comparison of Cr(VI) concentrations in the kinetic experiments of sorption with an**
417 **initial concentration of: (a) 4.8 × 10^{-5} mol L^{-1}; (b) 5.1 × 10^{-6} mol L^{-1} in contact with the reduced**
418 **sample (AUB00307) and the oxidized sample (AUB00976) of Tégulines Clay.**

419 4.5.3. *Boron*

420 Sorption experiments of B showed few differences between initial and final B concentrations in
421 solution (Fig. 11a). Experiments conducted at an initial concentration that is lower than the value
422 measured in equilibration tests (2.2 10^{-6} mol L^{-1}) would be expected to lead to higher final values than
423 the initial ones, confirming the high lability of B in our samples. In addition, the retention on both the
424 Teguline Clay were similar.

425

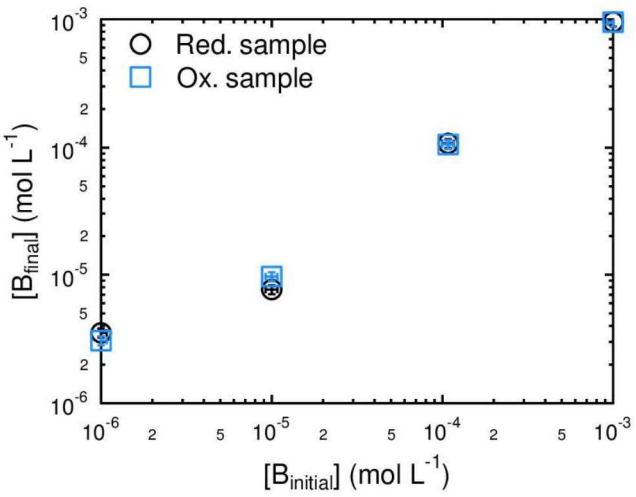

426

427 **Fig. 11. Initial and final B concentrations in sorption tests with the oxidized sample (AUB00976)**
428 **and the reduced sample (AUB009307) of Tégulines Clay.**

429 **5. Discussion**

430 5.1. Natural distribution coefficient ($R_{D,Nat}$) of As, Cr and B in the Tégulines Clay

431 This study revealed that As, Cr, and B are naturally present in the Tégulines Clay (in Reduced and
432 oxidized samples). These elements were released in the pore water in different amounts (Table 2)
433 depending on their abundance and the carrier phases. A natural element sediment-solution
434 partitioning coefficient called natural distribution coefficient ($R_{D,Nat}$) was calculated from those
435 measurements (Table 3) according to the equation 1:

436 $$R_{D,Nat} = \frac{C_{sediment,Nat}}{C_{pore\ water}} \quad \textbf{(1)}$$

437 where $C_{Pore\ water}$ is the pore water concentration of the toxic element in mol L^{-1} given in the Table 2, and
438 $C_{sediment,Nat}$ is the concentration of this toxic element in the sediments in mol kg^{-1} determined with the
439 sequential extractions (section 4.2).

440 High natural distribution coefficients were calculated for As and Cr (~2 10^4 L kg^{-1} for As, and ~7.5 10^4
441 L kg^{-1} for Cr), which confirm the affinity of those elements for the sediment phases in Tégulines Clay
442 (Table 3). In the meantime, the natural R_D of boron is three orders of magnitude lower (~60 L kg^{-1}),
443 and indicates the high lability of this element.

Table 3 Natural distribution coefficient $R_{D,Nat}$ in L kg^{-1} calculated with the pore water chemistry (mol L^{-1}) given in the Table 2 and the sediment natural concentration (mol kg^{-1}) in reduced and oxidized samples of Tégulines Clay determined with sequential extractions (section 4.2)

	As		Cr		B	
	oxidized	reduced	oxidized	reduced	oxidized	reduced
$C_{Pore\ water}$ (mol L^{-1})	$1.00\ 10^{-8}$	$1.00\ 10^{-8}$	$2.90\ 10^{-8}$	$2.90\ 10^{-8}$	$1.48\ 10^{-4}$	$1.48\ 10^{-4}$
$C_{sediment,Nat}$ (mol kg^{-1})	$2.83\ 10^{-4}$	$1.86\ 10^{-4}$	$1.48\ 10^{-3}$	$1.56\ 10^{-3}$	$1.29\ 10^{-3}$	$1.57\ 10^{-3}$
$R_{D,Nat}$ (L kg^{-1})	$1.9\ 10^{4}$	$2.8\ 10^{4}$	$7.4\ 10^{4}$	$7.8\ 10^{4}$	73	60

5.2. Influence of the labile fraction on the distribution coefficient (R_D)

The retention of an element of interest by a sediment was calculated through a distribution coefficient (R_D in L kg^{-1}), defined as the ratio between the concentration of the element sorbed on the sediment (C_{sorb} in mol kg^{-1}) over the element concentration remaining in the liquid (C_{final} in mol L^{-1}) according to Equation 2:

$$C_{sorb} = C_{final} R_D \quad \textbf{(2)}$$

However, the squeezing and equilibration experiments revealed that the three elements of interest present in the sediments were partly released in solution. Thus, the natural labile concentrations on the sediments ($C_{labile,ini}$ in mol kg^{-1}) must be considered in the calculation, depending on the results obtained during equilibration experiments. Therefore, C_{sorb} must be calculated according to Equation 3:

$$C_{sorb} = C_{labile,ini} + \frac{C_{added} - C_{final}}{R_{SL}} \quad \textbf{(3)}$$

where C_{added} is the added concentration in the retention experiments in mol L^{-1}, C_{final} is the element concentration at the end of the retention tests in mol L^{-1} and R_{SL} is the solid/liquid ratio in kg L^{-1}. This relationship modifies the distribution coefficient calculation, and is given by the relation 4:

$$R_D = \frac{C_{labile,ini} + \frac{(C_{added} - C_{final})}{R_{SL}}}{C_{final}} = \frac{R_{D_{ini}} C_{pore\ water} + \frac{(C_{added} - C_{final})}{R_{SL}}}{C_{final}} \quad \textbf{(4)}$$

where $C_{pore\ water}$ is the pore water measured by squeezing, and $R_{D,ini}$ is the initial R_D that considers the natural labile abundance of an element on the sediments. In the case of equilibration, C_{added} is equal to zero, so Equation 4 becomes:

$$R_{D,eq} = \frac{R_{D,ini} C_{pore\ water} - \frac{C_{final}}{R_{SL}}}{C_{final}} \quad \textbf{(5)}$$

Equations 4 and 5 are used to calculate the initial R_{Dini} that has to be considered for R_D calculations in the case of high labile concentrations of elements present in the clay rock such as B.

5.3. The role of natural abundance boron on its retention on Tégulines clay

The R_D calculations for B were influenced by B abundance in the sediments, because of the low natural R_D value. This R_D value reflects the high lability of this element *in situ*. However, B equilibration concentrations (~3 10^{-6} mol L^{-1} at R_{SL} = 10 g L^{-1}, Fig. 8) were fifty times lower than the pore water concentrations measured by squeezing (Table 2). With a water content of 0.15 and a R_{SL} of 0.01 kg L^{-1}, the contribution of pore water to the released B was 2.3 × 10^{-7} mol L^{-1}, or 8 times less than the equilibration concentration.

Consequently, B in solution originates mainly from desorption or from dissolution of a boron-bearing phase such as carbonates (Hemming and Hanson, 1992; Hemming et al., 1998; Mavromatis et al., 2015) or clay minerals (Muttik et al., 2011; Williams and Hervig, 2005). Because the squeezing method provides us with the equilibrium concentration after long interaction times that cannot be probed in laboratory experiments, the present observation indicates that B was mainly concentrated in phases that have very slow kinetics of equilibration with water (Fig. 7), consistent with concentration in the residual fraction. In addition, kinetic studies carried out on batch sorption experiments very frequently show two stages of uptake: an initial rapid uptake (minutes to hours) of the sorbing species, followed by a much slower uptake over the very long term. This behavior is generally interpreted as being the result of a two-stage process wherein a rapid adsorption reaction (ion exchange or surface complexation) is followed by a much slower process of sorbant incorporation into the solid matrix (by diffusion in the solid, solid-solution formation or co-precipitation). R_D values determined in batch systems on dispersed materials generally are based on the short-term sediment-solution partitioning values, and do not take into consideration the long-term evolution of the B concentrations.

491 The concentration of B in solution increased with the R_{SL} ratio in the equilibration experiments (Fig. 8).
492 In all cases, B concentrations remained lower than the total B quantity in the sediments (from 2 10^{-6} to
493 1 10^{-5} mol L^{-1}). Those equilibration experiments enabled calculation of an initial distribution coefficient
494 from the initial B concentration in the sediments, according to the relationship between B_{final} and R_{SL}. It
495 is noteworthy that the Milli-Q® water and analytical grade salts contained B. Thus, an additional term
496 had to be considered in the calculations, and the balance equation for boron became:

497 $$C_{Swater} + C_{labile,ini}R_{SL} + C_{pore\,water}w_{water}R_{SL} = C_{final} + C_{sorb}R_{SL} \quad \textbf{(6)}$$

498 where C_{Swater} is the element concentration in the synthetic solution once the analytical grade salts
499 were dissolved and w_{water} the water content. The relationship between the final concentration in the
500 experiment and the R_{Dinit} is obtained from Equations 2 and 6:

501 $$C_{final} = \frac{C_{Swater} + C_{labile,ini}R_{SL} + C_{pore\,water}w_{water}R_{SL}}{1 + R_{D,ini}R_{SL}} \quad \textbf{(7)}$$

502 Equation 7 and the equilibration experiments at several R_{SL} enabled $C_{labile,ini}$ and $R_{D,ini}$ for the two clay
503 samples to be determined (Fig. 8, Table 4).

504 **Table 4** Initial boron R_D (L kg^{-1}) and initial boron labile concentrations (molL^{-1}) in the two Tégulines Clay samples.
505 The calculation is made considering the water content (w_{water}), the boron concentration in the pore water (B_{poral}),
506 the boron concentration brought in solution by the Milli-Q® water and the salt (C_{Swater}) and the boron
507 concentration on the sediment ($C_{sediment}$).

	Reduced sample (AUB00307)	Oxidized sample AUB00976
w_{water} (L kg^{-1})	1.5 10^{-1}	1.5 10^{-1}
B_{poral} (mol L^{-1})	1.5 10^{-4}	1.5 10^{-4}
C_{Swater} (mol L^{-1})	2.1 10^{-6}	2.1 10^{-6}
$C_{sediment}$ (mol kg^{-1})	8.9 10^{-3}	1.1 10^{-2}
$R_{D,ini}$ (L kg^{-1})	6.0	6.0
$C_{labile,ini}$ (mol kg^{-1})	1.3 10^{-4}	7.5 10^{-5}

508

509 The labile concentration represents about 1 % of the total available boron in the sediments. In the
510 retention experiments on Tégulines Clay, R_{SL} was 0.01 kg L^{-1}. At this R_{SL}, the labile concentration
511 accounted for 40 % of the measured boron concentration in the reduced sample (AUB00307) and 28
512 % in the oxidized sample (AUB00976) in the equilibration experiments. Furthermore, the pore water

513 represented 18 % of this labile concentration in the reduced sample and 30 % in the oxidized sample.
514 The remaining part is explained by boron derived from the Milli-Q® water and the analytical grade
515 salts (Supplementary information D for detailed values).

516 $R_{D,ini}$ was then implemented in the Equation 4 to calculate the true R_D values, which considered the
517 added concentration and the natural abundance in the sediments (Fig. 12). C_{added} represented the
518 added B concentration plus the B concentration present in the synthetic solution. The R_D decrease
519 with the equilibrium concentration of boron was observed, except for the highest concentration. In that
520 case, the sorption was negligible compared to the added concentration. Those experiments showed
521 an initial saturation of the B sorption sites that exist on the sediments. For this reason, if the B natural
522 abundance was not considered, the R_D would have been lower than the calculated R_D or even
523 negative, if the final concentration were lower than the added concentration. The R_D values of the two
524 clay samples were similar, which indicates that the reducing capacity of the clay did not affect their
525 ability to retain B. This behavior is in a good agreement with the work of Goldberg et al. (2004) and
526 Hemming et al. (1998) which evidenced that B sorption capacity in rocks or soils mainly depends on
527 the organic matter, carbonate and iron oxi/hydroxide contents.

528 In our experiments, B uptake in calcite as observed in literature (Hemming and Hanson, 1992;
529 Hemming et al., 1998; Mavromatis et al., 2015) was rather limited because the solutions were initially
530 close to equilibrium with the mineralogical assemblage, yet slightly undersaturated. Consequently, the
531 carbonates were expected to dissolve slightly during the equilibration of the sediments with the
532 solution and release natural B. This may explain the high value of B content observed at the end of
533 some experiments. Finally, knowledge of the B natural background (abundance of an element) and its
534 lability are required to understand and explain its fate in the experiments.

535

536

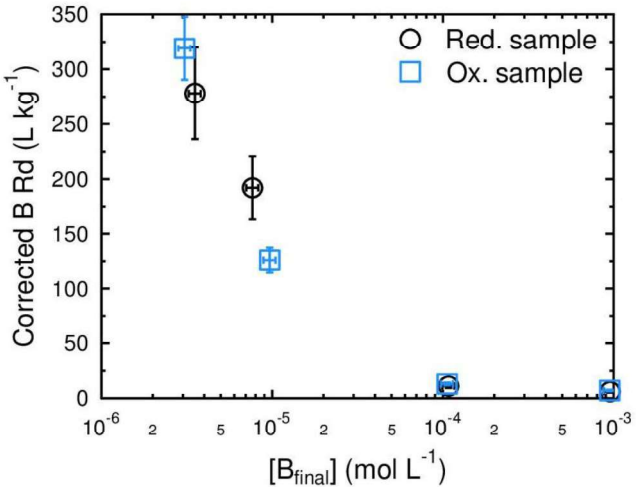

537

538 **Fig. 12. R_D (L kg^{-1}) corrected from the natural B in the Tégulines clay samples ($R_{D,ini}$ = 6 L kg^{-1}).**

539 *5.4. The role of redox on chromium retention on Tégulines Clay*

540 Under our measured conditions (pH = 7.4, pe = 6.8), Cr(III) was expected to be the predominant Cr
541 oxidation state, in the form of $HCrO_2$ or $Cr(OH)_3$, despite the oxidized conditions (Supplementary
542 information E) according to the Thermoddem or Thermochimie database were considered in the
543 calculations. However, the experimental conditions were close to the domain where Cr(VI) is
544 predominant as CrO_4^{2-}.

545 Cr speciation was strongly influenced by its interaction with the sediments. The reduced sample
546 efficiently reduced Cr(VI) to Cr(III) on the sediment, while the oxidized sample had a weaker influence
547 on Cr reduction. In any case, Cr(VI) was the only form of Cr detected in solution at the end of the
548 experiments.

549 EPMA analysis of the pristine rock revealed that Cr was closely associated to the glauconite.
550 However, Cr reduction can occur with Fe(II) derived from pyrite as well. This reduction operates even
551 in oxidizing conditions, because the Fe(II) oxidation by Cr(VI) is faster than by O_2 as demonstrated by
552 Eary and Rai (1989). Such reduction was previously demonstrated even under slight oxidizing
553 conditions, and with quantities 50 to 500 times greater than the amount of Cr(VI) introduced in our
554 reactors (Fendorf, 1995). This reduction caused Cr immobilization, leading to the formation of an
555 immobile coprecipitate with Cr(III), which stabilized the Cr (Markelova et al., 2018; Sass and Rai,
556 1987). Using geochemical calculations and the Cr concentration in squeezed pore water (2.9 10^{-8} mol

557 L^{-1}) in equilibrium with eskolaite (Cr_2O_3), chromite ($FeCr_2O_4$) or Cr hydroxide ($Cr(OH)_3$) commonly
558 found in natural environments (Manning et al., 2007; Pantsar-Kallio et al., 2001), the redox potential
559 was found to be equal to -118 mV (pe = -2), which is consistent with a predominant +III oxidation state
560 for Cr.

561 *5.5. The role of redox on arsenic retention on Tégulines Clay*

562 5.5.1. *As(III)*

563 We carried out sensitivity tests on the calculation of R_D for As(III) by varying the $R_{D,ini}$ value. Indeed As
564 concentration is independent of the solid/liquid ratio (section 4.4), therefore $C_{labile,ini}$ and $R_{D,ini}$ cannot be
565 determined according to the equation 7 as realized for B. In addition, As was poorly labile compared to
566 B, as demonstrated by the equilibration tests (Fig. 7) and the natural R_D (Table 4). Therefore, there
567 were few differences between the R_D calculated from Equation 1 and the R_D calculated considering
568 the As labile fraction using Equation 5 (Table 5). In addition, no As(III) oxidation in As(V) were
569 observed in solution.

570 **Table 5** Influence of the $R_{D,ini}$ on the distribution coefficient (R_D) calculated for As(III) sorption experiments. The
571 calculations with the R_{Dini} correction were done with the equation 5 while the calculation without correction were
572 done with the equation 1.

			R_{Dini} (L kg^{-1})		
			200	500	1000
	C_{final} (mol L^{-1})	R_D without correction (L kg^{-1})	R_D with correction		
Reduced (AUB00307)	$9.18 \cdot 10^{-7}$	90	93	96	101
	$1.01 \cdot 10^{-5}$	74	74	74	75
	$1.17 \cdot 10^{-4}$	33	33	33	33
	$1.36 \cdot 10^{-3}$	16	16	16	16
Oxidized (AUB00976)	$7.46 \cdot 10^{-7}$	132	135	139	145
	$8.73 \cdot 10^{-6}$	100	100	100	101
	$1.07 \cdot 10^{-4}$	45	45	45	45
	$1.29 \cdot 10^{-3}$	22	22	22	22

573

574 The $R_{D,ini}$ value was constrained by the equilibration tests and the squeezing results. In contrast to B,
575 the two values were similar (~10^{-8} mol L^{-1}), and thus by considering an $R_{D,ini}$ equal to 100 L kg^{-1},

576 $C_{labile,ini}$ was 10^{-6} mol kg^{-1}. This As(III) quantity was diluted in the equilibration experiments (10^{-8} mol L^{-1}) and was allocated equally between the measured concentration in solution (~0.5 × 10^{-8} mol L^{-1}) and the sediments. That quantity on the sediments is consistent with the assumed $R_{D,ini}$, according to the Equation 1 (0.5 10^{-8} × 100 × 0.01 = 0.5 10^{-8} mol L^{-1}). Finally, As(III) retention and the natural concentrations measured by squeezing and equilibration were explained by a reversible adsorption mechanism.

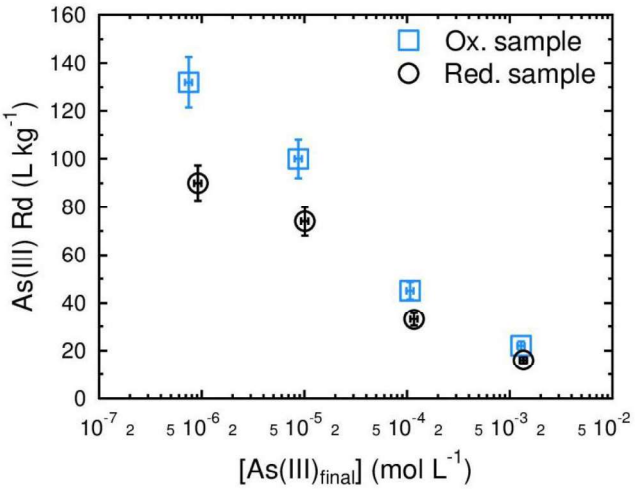

582

583 **Fig. 13. Comparison of the retention values obtained for As(III) on the oxidized sample**
584 **(AUB00976) and on the reduced sample (AUB00307), based on the squeezed pore water**
585 **concentration (1 10^{-8} mol L^{-1}).**

586 5.5.2. *As(V) case*

587 Significant As(III) concentrations were measured in solution during the As(V) retention experiments
588 (see Section 4.5). The distribution coefficient previously calculated for As(III) (see Section 5.5.1) for
589 each Tégulines Clay enabled calculation of the As(III) labile concentration on the sediments according
590 to Equation 2. The total concentration of As(V) reduced to As(III) was then calculated with this labile
591 concentration on the sediments and the concentration in solution (Equation 8). Finally, the sorbed
592 concentration of the As(V) can be corrected from the contribution of As(III) (see Supplementary
593 information F for details). This concentration permitted calculation of the distribution coefficient of
594 As(V) (Equation 9) on the two samples of Tégulines Clay (Fig. 14).

595 $$[As(V)]_{reduced} = [As(III)]_{labile} + [As(III)]_{final} \quad \textbf{(8)}$$

596 $$R_{D,As(V)} = \frac{[As(V)]_{ini} - [As(V)]_{final} - [As(V)]_{reduced}}{[As(V)]_{final}} \quad \textbf{(9)}$$

597 In contrast to Cr(VI), the R_D for As(V) were almost identical for the reduced and oxidized samples.
598 Thus, by analogy with Cr(VI), As(V) was reduced to As(III) by the sediments, albeit the degree of
599 reduction was much lower. It is noteworthy that the hypothesis of As(V) reduction on the sediments is
600 consistent with the As(III) release in solution observed in the equilibration tests (see Section 4.4).

601 As(III) R_D can be compared to the As(V) R_D obtained after 7 days of equilibration. From this
602 comparison, it appears that the As(V) R_D was higher than that of As(III) (Fig. 14), consistent with
603 previous studies (Goldberg and Johnston, 2001; Liu et al., 2001; Verbeeck et al., 2017) and its high
604 affinity for Fe and Mn oxyhydroxides (Wu et al., 2018). In addition, the R_D of As(III) was higher on the
605 oxidized sample than on the reduced sample, consistent with the observed presence of Fe
606 oxyhydroxides in the sample collected near the surface, which have high affinity for As(III) (Daus et al.,
607 1998; Frommer et al., 2011; Giménez et al., 2007).

608 The reduction of As(V) into As (III) on the sediments made impossible the determination of an
609 adsorption coefficient for As(V). However, the retention experiments involving As(III) enabled the
610 deconvolution of the mechanisms involved in the As retention in the Tégulines Clay. Without this
611 information, it would have been impossible to distinguish the sorbed As(V) from the As(V) that was
612 reduced and then sorbed as As(III). The redox potential processes make the R_D of As dependent on
613 the mineralogy of the sample and on the solid/liquid ratio.

614 As shown by the EPMA analyses of pristine rock, As was essentially carried by pyrite in the reduced
615 sample (Fig. 4). Furthermore, electron microprobe analyses made on pristine samples revealed an
616 enrichment of the iron oxide formed by the oxidation of pyrite compared to the iron hydroxides in the
617 clay matrix. Thus, the presence of Fe oxyhydroxides enhanced the retention of the added As on the
618 samples (Goldberg, 2002; Goldberg and Johnston, 2001).

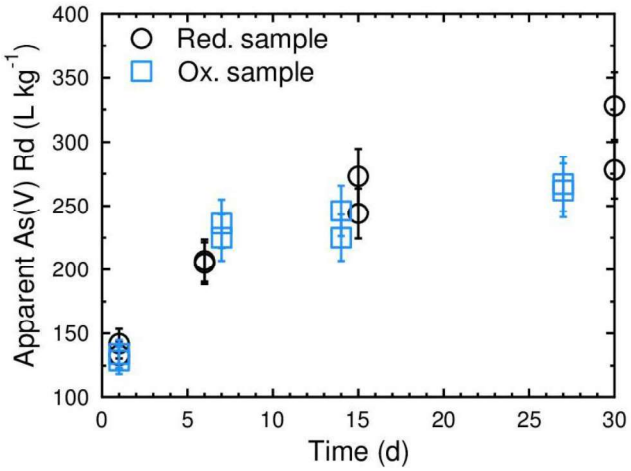

Fig. 14. Apparent As(V) R_D values corrected from the As(III) reduced on the sediments in contact with the reduced sample (AUB00307) and the oxidized sample (AUB00976). The two dots for a same time are replicates.

6. Conclusions

The behavior of As, Cr, and B retention has been investigated in Tégulines Clay, an outcropping clay-rich rock formation. The retention of the studied oxyanions was affected by the clay mineralogy (As, Cr and B), their natural abundance (B), and the reducing capacity of the samples (As and Cr). Cr(VI) oxyanion (CrO_4^{2-}) was immobilized by its reduction on the sediments. The reduction was more effective in the reduced sample than in the oxidized sample. Such reduction also occurs to a lesser extent for As(V). $HAsO_4^{2-}$ and AsO_2^-, which are As(V) and As(III) oxyanions, were retained by their sorption on the positively charged mineral surfaces. As(III) was retained slightly more in the oxidized sample (AUB00976) than in the reduced sample (AUB00307), due to presence of Fe oxyhydroxides on which is preferably sorbed. The sorption sites of the samples were initially saturated with B and could not retain additional $B(OH)_4^-$. Any analysis of B lability needs to consider its natural occupancy to avoid an underestimation of the sorption capacities of B on the samples. This abundance is usually excluded from the distribution coefficient calculations, mostly on the basis of the low initial B contents. This study demonstrates that B natural abundance can strongly influence the distribution calculations. We proposed a methodology for the estimation of the retention properties of weakly adsorbed species on natural sediment. This methodology makes it possible to obtain accurate distribution coefficients that are useful for the prediction of the mobility of toxic chemicals in order to support the assessment of the environmental impact of a LL-LL radioactive waste repository.

Acknowledgements

This research was financially supported by the BRGM–Andra scientific partnership (TOGAULT project). Thank you to Michel Fialin (IPGP, Camparis) for his support with the electron microprobe mapping. We would like to thank Editage (www.editage.com) for English language editing.

646

647 **References**

648 Adriano DC. Trace elements in the terrestrial environment. New York: Springer-Verlag, 1986.

649 Alloway B. Soil processes and the behavior of metals. Heavy metals in soils 1995; 2: 11-37.

650 Amédro F, Matrion B, Deconinck J-F, Huret E, Landrein P. Les forages de Juzanvigny (Aube, France):
651 litho-biostratigraphie des formations du Barrémien à l'Albien moyen dans l'est du bassin de
652 Paris et datations par les ammonites. Geodiversitas 2017; 39: 185-212.

653 Arai Y. Arsenic and Antimony. In: Hooda P, S., editor. Trace Elements in Soils. Wiley, London, 2010,
654 pp. 618.

655 Bartlett R, James B. Behavior of Chromium in Soils: III. Oxidation1. Journal of Environmental Quality
656 1979; 8: 31-35.

657 Blanc P, Lassin A, Piantone P, Azaroual M, Jacquemet N, Fabbri A, et al. Thermoddem: A
658 geochemical database focused on low temperature water/rock interactions and waste
659 materials. Applied Geochemistry 2012; 27: 2107-2116.

660 Claret F, Lerouge C, Laurioux T, Bizi M, Conte T, Ghestem JP, et al. Natural iodine in a clay formation:
661 Implications for iodine fate in geological disposals. Geochimica et Cosmochimica Acta 2010;
662 74: 16-29.

663 Couch EL, Grim RE. Boron fixation by illites. Clays Clay Miner 1968; 16.

664 Daus B, Weiß H, Wennrich R. Arsenic speciation in iron hydroxide precipitates. Talanta 1998; 46: 867-
665 873.

666 Eary LE, Rai D. Kinetics of chromate reduction by ferrous ions derived from hematite and biotite at
667 25°C. Am. J. Sci. 1989; 289: 180-213.

668 Evans LJ. Chemistry of metal retention by soils. Environmental Science & Technology 1989; 23: 1046-
669 1056.

670 Fendorf S, Eick MJ, Grossl P, Sparks DL. Arsenate and Chromate Retention Mechanisms on
671 Goethite. 1. Surface Structure. Environmental Science & Technology 1997; 31: 315-320.

672 Fendorf SE. Surface reactions of chromium in soils and waters. Geoderma 1995; 67: 55-71.

673 Fernández AM, Sánchez-Ledesma DM, Tournassat C, Melón A, Gaucher EC, Astudillo J, et al.
674 Applying the squeezing technique to highly consolidated clayrocks for pore water
675 characterisation: Lessons learned from experiments at the Mont Terri Rock Laboratory.
676 Applied Geochemistry 2014; 49: 2-21.

677 Fleet M. Preliminary investigations into the sorption of boron by clay minerals. Clay Miner 1965; 6: 3-
678 16.

679 Frommer J, Voegelin A, Dittmar J, Marcus MA, Kretzschmar R. Biogeochemical processes and
680 arsenic enrichment around rice roots in paddy soil: results from micro-focused X-ray
681 spectroscopy. European Journal of Soil Science 2011; 62: 305 - 317.

682 Gaucher EC, Tournassat C, Pearson FJ, Blanc P, Crouzet C, Lerouge C, et al. A robust model for
683 pore-water chemistry of clayrock. Geochimica et Cosmochimica Acta 2009; 73: 6470-6487.

684 Giffaut E, Grivé M, Blanc P, Vieillard P, Colàs E, Gailhanou H, et al. Andra thermodynamic database
685 for performance assessment: ThermoChimie. Applied Geochemistry 2014; 49: 225-236.

686 Giménez J, Martínez M, de Pablo J, Rovira M, Duro L. Arsenic sorption onto natural hematite,
687 magnetite, and goethite. Journal of Hazardous Materials 2007; 141: 575-580.

688 Goldberg S. Reactions of boron with soils. Plant and Soil 1997; 193: 35-48.

689 Goldberg S. Competitive adsorption of arsenate and arsenite on oxides and clay minerals. Soil Sci.
690 Soc. Am. J. 2002; 66: 413–421.

691 Goldberg S, Johnston CT. Mechanisms of Arsenic Adsorption on Amorphous Oxides Evaluated Using
692 Macroscopic Measurements, Vibrational Spectroscopy, and Surface Complexation Modeling.
693 Journal of Colloid and Interface Science 2001; 234: 204-216.

694 Goldberg S, Suarez DL. Role of Organic Matter on Boron Adsorption-Desorption Hysteresis of Soils.
695 Soil Science 2012; 177: 417-423.

696 Goldberg S, Suarez DL, Basta NT, Lesch SM. Predicting Boron Adsorption Isotherms by Midwestern
697 Soils using the Constant Capacitance Model. Soil Science Society of America Journal 2004;
698 68: 795-801.

699 Gorny J, Billon G, Lesven L, Dumoulin D, Madé B, Noiriel C. Arsenic behavior in river sediments under
700 redox gradient: A review. Science of The Total Environment 2015; 505: 423-434.

701 Gorny J, Billon G, Noiriel C, Dumoulin D, Lesven L, Madé B. Chromium behavior in aquatic
702 environments: a review. Environmental Reviews 2016; 24: 503-516.

703 Gran G. Determination of the equivalence point in potentiometric titrations. Part II. Analyst 1952; 77:
704 661-671.

705 Gulens J, Champ DR, Jackson RE. Influence of redox environments on the mobility of arsenic in
706 ground water. Am. Chem. Soc. Symp. Ser. 1979; 93: 81-95.

707 Hemming NG, Hanson GN. Boron isotopic composition and concentration in modern marine
708 carbonates. Geochimica et Cosmochimica Acta 1992; 56: 537-543.

709 Hemming NG, Reeder RJ, Hart SR. Growth-step-selective incorporation of boron on the calcite
710 surface. Geochimica et Cosmochimica Acta 1998; 62: 2915-2922.

711 Jain A, Loeppert RH. Effect of competing anions on the adsorption of arsenate and arsenite by
712 ferrihydrite. J. Environ. Qual. 2000; 29: 1422–1430.

713 James BR, Bartlett RJ. Behavior of Chromium in Soils. VI. Interactions Between Oxidation-Reduction
714 and Organic Complexation1. Journal of Environmental Quality 1983a; 12: 173-176.

715 James BR, Bartlett RJ. Behavior of Chromium in Soils: V. Fate of Organically Complexed Cr(III) Added
716 to Soil1. Journal of Environmental Quality 1983b; 12: 169-172.

717 Lerouge C, Robinet J-C, Debure M, Tournassat C, Bouchet A, Fernández AM, et al. A Deep Alteration
718 and Oxidation Profile in a Shallow Clay Aquitard: Example of the Tégulines Clay, East Paris
719 Basin, France. Geofluids 2018: 20.

720 Li Z. Oxyanion Sorption and Surface Anion Exchange by Surfactant-Modified Clay Minerals. Journal of
721 Environmental Quality 1999; 28: 1457-1463.

722 Li Z, Bowman RS. Retention of inorganic oxyanions by organo-kaolinite. Water Research 2001; 35:
723 3771-3776.

724 Liu SX, Athar M, Lippai I, Waldren C, Hei TK. Induction of oxyradicals by arsenic: Implication for
725 mechanism of genotoxicity. Proceedings of the National Academy of Sciences 2001; 98:
726 1643-1648.

727 Lynch S, Batty L, Byrne P. Environmental Risk of Metal Mining Contaminated River Bank Sediment at
728 Redox-Transitional Zones. Minerals 2014; 4: 52-73.

729 Ma Y, Hooda PS. Chromium, Nickel and Cobalt. In: Hooda PS, editor. Trace Elements in Soils. Wiley,
730 London, 2010, pp. 618.

731 Manning BA, Kiser JR, Kwon H, Kanel SR. Spectroscopic Investigation of Cr(III)- and Cr(VI)-Treated
732 Nanoscale Zerovalent Iron. Environmental Science & Technology 2007; 41: 586-592.

733 Markelova E, Couture R-M, Parsons CT, Markelov I, Madé B, Van Cappellen P, et al. Speciation
734 dynamics of oxyanion contaminants (As, Sb, Cr) in argillaceous suspensions during oxic-
735 anoxic cycles. Applied Geochemistry 2018.

736 Masscheleyn PH, Delaune RD, Patrick WH. Effect of redox potential and pH on arsenic speciation and
737 solubility in a contaminated soil. Environmental Science & Technology 1991; 25: 1414-1419.

738 Mavromatis V, Montouillout V, Noireaux J, Gaillardet J, Schott J. Characterization of boron
739 incorporation and speciation in calcite and aragonite from co-precipitation experiments under
740 controlled pH, temperature and precipitation rate. Geochimica et Cosmochimica Acta 2015;
741 150: 299-313.

742 Muttik N, Kirsimäe K, Newsom HE, Williams LB. Boron isotope composition of secondary smectite in
743 suevites at the Ries crater, Germany: boron fractionation in weathering and hydrothermal
744 processes. Earth and Planetary Science Letters 2011; 310: 244-251.

745 Nagajyoti PC, Lee KD, Sreekanth TVM. Heavy metals, occurrence and toxicity for plants: a review.
746 Environ Chem Lett 2010; 8: 199-216.

747 Nakayama E, Tokoro H, Kuwamoto T, Fujinaga T. Dissolved state of chromium in seawater. Nature
748 1981; 290: 768-770.

749 Pantsar-Kallio M, Reinikainen S-P, Oksanen M. Interactions of soil components and their effects on
750 speciation of chromium in soils. Analytica Chimica Acta 2001; 439: 9-17.

751 Parkhurst DL, Appelo CAJ. Description of Input and Examples for PHREEQC Version 3–a Computer
752 Program for Speciation, Batch-reaction, One-dimensional Transport, and Inverse
753 Geochemical Calculations., 2013.

754 Penrose WR. Arsenic in the marine and aquatic environments: Analysis, occurrence, and significance.
755 CRC Crit. Rev. Environ. Control 1974; 4: 465–482.

756 Poggio L, Vrščaj B, Schulin R, Hepperle E, Ajmone Marsan F. Metals pollution and human
757 bioaccessibility of topsoils in Grugliasco (Italy). Environmental Pollution 2009; 157: 680-689.

758 Pouchou JL, Pichoir F. New model for quantitative x-ray microanalysis. Part I: Application to the
759 analysis of homogeneous samples [English Ed.]. Vol 3, 1984.

760 Sass BM, Rai D. Solubility of amorphous chromium(III)-iron(III) hydroxide solid solutions. Inorganic
761 Chemistry 1987; 26: 2228-2232.

762 Smedley PL, Kinniburgh DG. A review of the source, behaviour and distribution of arsenic in natural
763 waters. Applied Geochemistry 2002; 17: 517-568.

764 Sparks DL. Metal and Oxyanion Sorption on Naturally Occurring Oxide and Clay Mineral Surfaces. In:
765 Grassian V, H., editor. Environmental Catalysis, 2005, pp. 3–36.

766 Taghipour M, Jalali M. Effect of clay minerals and nanoparticles on chromium fractionation in soil
767 contaminated with leather factory waste. Journal of Hazardous Materials 2015; 297: 127-133.

768 Tallman DE, Shaikh AU. Redox stability of inorganic arsenic(III) and arsenic(V) in aqueous solution.
769 Analytical Chemistry 1980; 52: 196-199.

770 Tessier A, Campbell PGC, Bisson M. Sequential extraction procedure for the speciation of particulate
771 trace metals. Analytical Chemistry 1979; 51: 844-851.

772 Verbeeck M, Hiemstra T, Thiry Y, Smolders E. Soil organic matter reduces the sorption of arsenate
773 and phosphate: a soil profile study and geochemical modelling. European Journal of Soil
774 Science 2017; 68: 678-688.

775 Walsh LM, Keeney DR. Behavior and Phototoxicity of Inorganic Arsenicals in Soils. Arsenical
776 Pesticides. 7. AMERICAN CHEMICAL SOCIETY, 1975, pp. 35-52.

777 Wauchope RD, McDowell. LL. Adsorption of phosphate, arsenate, methanearsonate, and cacodylate
778 by lake and stream sediments: Comparisons with soils. J. Environ. Qual. 1984; 13: 499–504.

779 Williams LB, Hervig RL. Lithium and boron isotopes in illite-smectite: The importance of crystal size.
780 Geochimica et Cosmochimica Acta 2005; 69: 5705-5716.

781 Wu Y, Kukkadapu RK, Livi KJT, Xu W, Li W, Sparks DL. Iron and Arsenic Speciation During As(III)
782 Oxidation by Manganese Oxides in the Presence of Fe(II): Molecular-Level Characterization
783 Using XAFS, Mössbauer, and TEM Analysis. ACS Earth and Space Chemistry 2018.

784 Wuana RA, Okieimen FE. Heavy Metals in Contaminated Soils: A Review of Sources, Chemistry,
785 Risks and Best Available Strategies for Remediation. ISRN Ecology 2011; 2011: 20.

786 Zhang G, Germaine JT, Martin RT, Whittle AJ. A simple sample-mounting method for radndom
787 powder X-ray diffraction. Clays and Clay Minerals 2003; 51: 218-225.

788

789

790 **Supplementary files**

791 **Supplementary information A. Sequential extraction steps and mineralogical targets**

792

793 **Table A-1. Chemical extraction scheme for As, Cr and B fractionation.**

Step	Extractant	Mineralogical target
1	$MgCl_2$ 1 M	Interfoliar exchange in clay minerals
2	Sodium acetate / Acetic acid (pH 5)	Calcite and clay edge sites
3	NH_2OH	Iron and manganese oxyhydroxides
4	H_2O_2 30 % + ammonium acetate (pH 2 at 85°C)	Organic matter

794

795

796

797 **Supplementary information B. Synthetic water composition and analytical grade salts**

798

799 **Table B-1. Synthetic water composition in mol L^{-1} given in element.**

Element	Ca	Na	Mg	K	Sr	HCO_3^-	Cl	SO_4
Concentration (mol L^{-1})	$3.09\ 10^{-3}$	$2.43\ 10^{-3}$	$1.94\ 10^{-3}$	$6.70\ 10^{-4}$	$2.50\ 10^{-4}$	$3.16\ 10^{-3}$	$1.56\ 10^{-3}$	$4.44\ 10^{-3}$

800

801

802 **Table B-2. Analytical grade salt used to prepare synthetic water and their weight (mg L^{-1}) and**
803 **molar (mol L^{-1}) concentrations.**

Salt	Molar mass (g mol^{-1})	Weight concentration (mg L^{-1})	Molar concentration (mol L^{-1})
$CaCO_3 \cdot 2\ H_2O$	118.1	7.1	$6.01\ 10^{-5}$
$SrCl_2 \cdot 6\ H_2O$	266.6	66.7	$2.50\ 10^{-4}$
$MgCl_2$	95.2	50.5	$5.30\ 10^{-4}$
$MgSO_4$	120.4	169.7	$1.41\ 10^{-3}$
$CaSO_4$	136.1	412.5	$3.03\ 10^{-3}$
$NaHCO_3$	84	204.1	$2.43\ 10^{-3}$
$KHCO_3$	100.1	67.1	$6.70\ 10^{-4}$

804

805

806

807 **Supplementary information C. Results of As(III) sorption on the Tegulines Clay**

808

809 **Figure C-1. Initial and final As(III) concentrations in sorption tests with the oxidized sample**
810 **(AUB00976) and the reduced sample (AUB009307) of Tégulines Clay.**

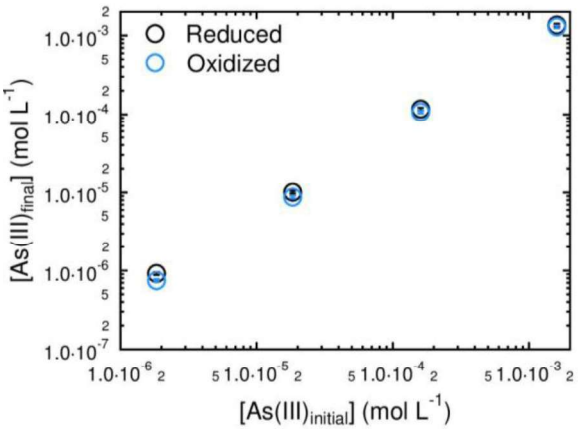

811

812

813

814 **Supplementary information D. Parameters for the determination of the boron $R_{D,ini}$, $C_{labile,ini}$ and**
815 **concentrations repartition (labile, sediment, poral, salt, Milli-Q® water).**

816

817 **Table D-1. Initial boron R_D, initial boron labile concentrations, percentage of each end member**
818 **in the boron concentrations of the two samples of Tégulines Clay**

	Reduced sample (AUB00307)	Oxidized sample (AUB00976)
w_{water} (L kg^{-1})	$1.5\ 10^{-1}$	$1.5\ 10^{-1}$
B_{poral} (mol L^{-1})	$1.5\ 10^{-4}$	$1.5\ 10^{-4}$
C_{Swater} (mol L^{-1})	$2.1\ 10^{-6}$	$2.1\ 10^{-6}$
$C_{sediment}$ (mol kg^{-1})	$8.9\ 10^{-3}$	$1.1\ 10^{-2}$
$R_{D,ini}$ (L kg^{-1})	6.0	6.0
$C_{labile,ini}$ (mol kg^{-1})	$1.3\ 10^{-4}$	$7.5\ 10^{-5}$
$C_{labile,ini}$ (mol L^{-1})	$1.3\ 10^{-6}$	$7.5\ 10^{-7}$
C_{final} (mol L^{-1})	$3.1\ 10^{-6}$	$2.7\ 10^{-6}$
$C_{labille}$ / $C_{sediment}$ (%)	1.4	0.7
$C_{labille}$ / C_{final} (%)	40.1	27.7
B_{poral} / C_{labile} (%)	17.8	29.6

819

820

821

822 **Supplementary information E. Chromium stability diagrams**

823

824 **Figure E-1. Cr stability diagram calculated using the Tégulines pore water chemistry**
825 **determined by squeezing (Lerouge et al., 2018) and the Thermoddem database (Blanc et al.,**
826 **2012): (a) aqueous species; (b) chromite; (c) eskolaite; (d) aqueous species with ThermoChimie**
827 **database (Giffaut et al., 2014). $Cr(OH)_3$ was undersaturated in those conditions. Measured and**
828 **estimated pe/pH domains (see section 5.4) are highlighted on the diagrams.**

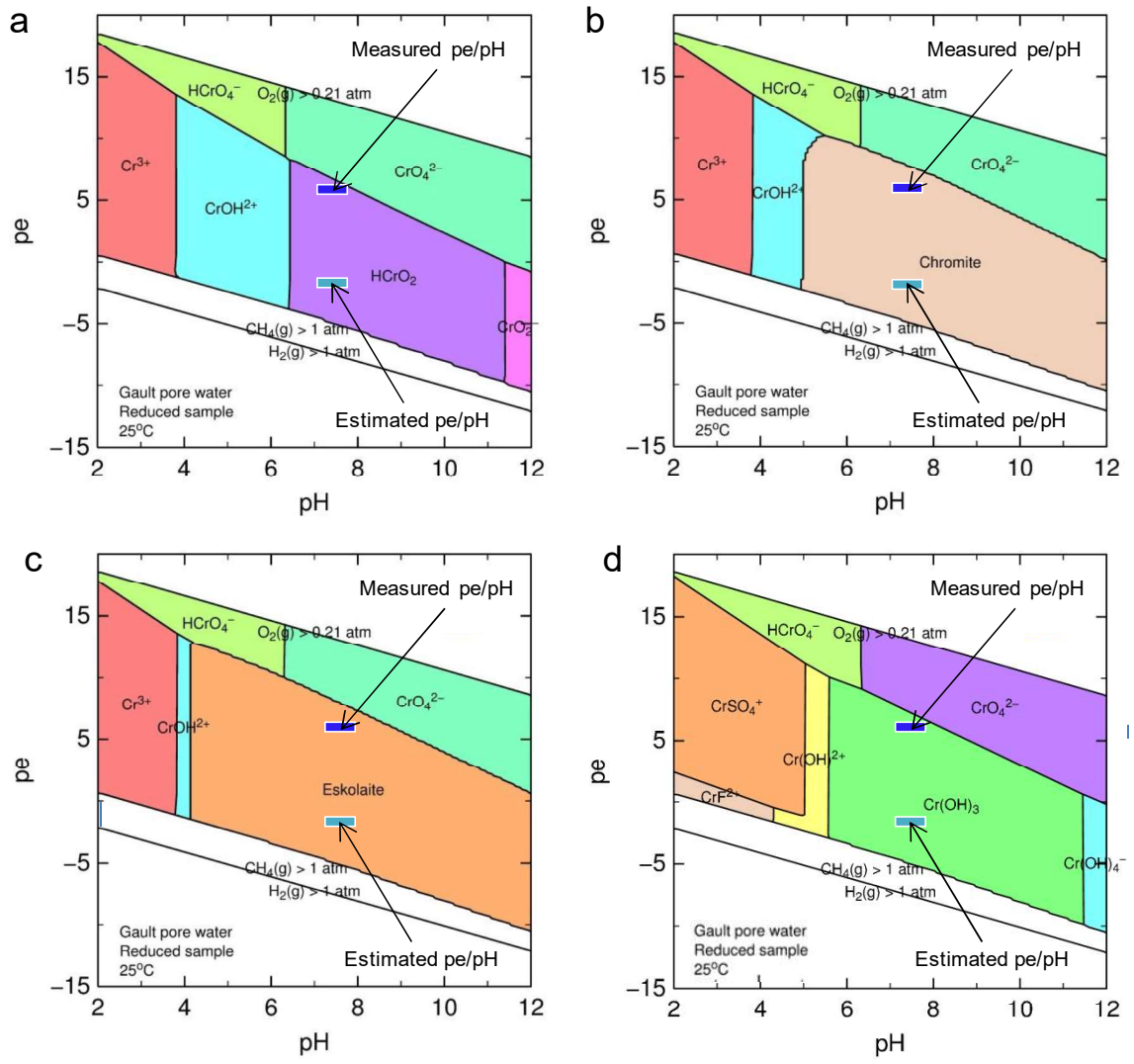

829

830

831

832 **Supplementary informationSupplementary information F. Determination of the total reduced**
833 **As(III) on the sediment in the sorption experiments**

834

835 **Table F-1. Case of the reduced sample (AUB00307)**

$As(III)_{final}$ (mol L^{-1})	R_D ($L \cdot kg^{-1}$)	$As(III)_{labile}$ ($mol \cdot kg^{-1}$)	$As(V)_{reduced}$ ($mol \cdot L^{-1}$)	$As(V)_{final}$ ($mol \cdot L^{-1}$)	$As(V)_{sorb}$ ($mol \cdot kg^{-1}$)
$1.45 \cdot 10^{-6}$	$9.04 \cdot 10^{1}$	$1.32 \cdot 10^{-4}$	$2.78 \cdot 10^{-6}$	$9.33 \cdot 10^{-6}$	$1.32 \cdot 10^{-3}$
$7.31 \cdot 10^{-7}$	$9.04 \cdot 10^{1}$	$6.61 \cdot 10^{-5}$	$1.42 \cdot 10^{-6}$	$7.60 \cdot 10^{-6}$	$1.58 \cdot 10^{-3}$
$1.42 \cdot 10^{-6}$	$9.04 \cdot 10^{1}$	$1.29\ 10^{-4}$	$2.71 \cdot 10^{-6}$	$6.08 \cdot 10^{-6}$	$1.66 \cdot 10^{-3}$
$6.38 \cdot 10^{-7}$	$9.04 \cdot 10^{1}$	$5.77 \cdot 10^{-5}$	$1.23 \cdot 10^{-6}$	$6.25 \cdot 10^{-6}$	$1.74 \cdot 10^{-3}$
$1.00 \cdot 10^{-6}$	$9.04 \cdot 10^{1}$	$9.05 \cdot 10^{-5}$	$1.94 \cdot 10^{-6}$	$9.86 \cdot 10^{-6}$	$1.31 \cdot 10^{-3}$
$8.41 \cdot 10^{-7}$	$9.04 \cdot 10^{1}$	$7.60 \cdot 10^{-5}$	$1.64 \cdot 10^{-6}$	$7.54 \cdot 10^{-6}$	$1.55 \cdot 10^{-3}$
$4.83 \cdot 10^{-7}$	$9.04 \cdot 10^{1}$	$4.37 \cdot 10^{-5}$	$9.35 \cdot 10^{-7}$	$6.92 \cdot 10^{-6}$	$1.69 \cdot 10^{-3}$
$6.22 \cdot 10^{-7}$	$9.04 \cdot 10^{1}$	$5.62 \cdot 10^{-5}$	$1.21 \cdot 10^{-6}$	$5.48 \cdot 10^{-6}$	$1.80 \cdot 10^{-3}$

836

837

838 **Table F-2. Case of the oxidized sample (AUB00976)**

$As(III)_{final}$ (mol L^{-1})	R_D ($L \cdot kg^{-1}$)	$As(III)_{labile}$ ($mol \cdot kg^{-1}$)	$As(V)_{reduced}$ ($mol \cdot L^{-1}$)	$As(V)_{final}$ ($mol \cdot L^{-1}$)	$As(V)_{sorb}$ ($mol \cdot kg^{-1}$)
$2.00 \cdot 10^{-6}$	$1.32 \cdot 10^{2}$	$2.64 \cdot 10^{-4}$	$4.69 \cdot 10^{-6}$	$8.84 \cdot 10^{-6}$	$1.16 \cdot 10^{-3}$
$1.43 \cdot 10^{-6}$	$1.32 \cdot 10^{2}$	$1.89 \cdot 10^{-4}$	$3.33 \cdot 10^{-6}$	$6.57 \cdot 10^{-6}$	$1.54 \cdot 10^{-3}$
$5.39 \cdot 10^{-7}$	$1.32 \cdot 10^{2}$	$7.12 \cdot 10^{-5}$	$1.26 \cdot 10^{-6}$	$6.90 \cdot 10^{-6}$	$1.70 \cdot 10^{-3}$
$1.55 \cdot 10^{-6}$	$1.32 \cdot 10^{2}$	$2.04 \cdot 10^{-4}$	$3.59 \cdot 10^{-6}$	$6.05 \cdot 10^{-6}$	$1.58 \cdot 10^{-3}$
$2.13 \cdot 10^{-6}$	$1.32 \cdot 10^{2}$	$2.81 \cdot 10^{-4}$	$4.98 \cdot 10^{-6}$	$8.96 \cdot 10^{-6}$	$1.13 \cdot 10^{-3}$
$9.88 \cdot 10^{-7}$	$1.32 \cdot 10^{2}$	$1.30 \cdot 10^{-4}$	$2.30 \cdot 10^{-6}$	$7.05 \cdot 10^{-6}$	$1.59 \cdot 10^{-3}$
$9.32 \cdot 10^{-7}$	$1.32 \cdot 10^{2}$	$1.23 \cdot 10^{-4}$	$2.18 \cdot 10^{-6}$	$7.08 \cdot 10^{-6}$	$1.59 \cdot 10^{-3}$
$1.76 \cdot 10^{-6}$	$1.32 \cdot 10^{2}$	$2.32 \cdot 10^{-4}$	$4.10 \cdot 10^{-6}$	$5.81 \cdot 10^{-6}$	$1.53 \cdot 10^{-3}$

839

840